Article published with copyright in
International Materials Reviews 2009 Vol. 54 No. 2.

Intermediate Temperature Embrittlement of Copper Alloys

V. Laporte* and A. Mortensen

vincent.laporte@epfl.ch
andreas.mortensen@epfl.ch

Ecole Polytechnique Fédérale de Lausanne (EPFL),
Laboratory for Mechanical Metallurgy, Institute of Materials
Station 12, CH-1015 Lausanne, Switzerland

* *now at:*
vincent.laporte@alcan.com
Alcan Engineered Products, Voreppe Research Centre (CRV), Melting and Casting Unit
Parc Economique Centr'Alp - BP 27, F - 38341 Voreppe Cedex, France

ABSTRACT

Copper and its alloys generally display a severe reduction in ductility between roughly 300°C and 600°C, a phenomenon variously called "intermediate temperature embrittlement" or "ductility trough behaviour". This review of the phenomenon begins by placing it in the wider context of the high-temperature fracture of metals, showing how its occurrence can be rationalized in simple terms on the basis of what is known of intergranular creep fracture and dynamic recrystallisation. Data in the literature are reviewed to identify main causes and mechanisms for embrittlement, first for pure copper, and then for monophase and multiphase copper alloys. Coverage then turns to the "grain boundary embrittlement" phenomenon, caused by the intergranular segregation of even minute quantities of alloying additions or impurities, which appears to worsen dramatically the intermediate temperature embrittlement of copper alloys. Finally, metal-induced embrittlement, including in particular liquid metal embrittlement, is presented as a second mechanism leading to an exacerbation of the intermediate temperature embrittlement of copper and its alloys.

Keywords: copper, ductility, intergranular fracture, grain boundary embrittlement, liquid metal embrittlement, creep fracture, solid metal embrittlement, dynamic embrittlement.

PLAN OF THE ARTICLE

Introduction

Copper and copper alloys do not display a regular evolution in their mechanical properties as temperature increases. Their yield stress and hardness decrease monotonously but their ductility generally goes through a minimum, exhibiting a sharp decrease around 300°C before rising again and then exceeding room temperature values. The effect is most often quantified by means of tensile data plotted versus temperature: it then appears as a sharp decrease, over a limited temperature range, of both the tensile elongation to failure and the reduction in area at fracture. Other tests can however also reveal the effect: the ductility minimum appears thus in impact energy absorption[1, 2] or hot torsion[3] data. This type of behaviour, which has wide-ranging consequences in industrial practice, is often termed "ductility trough behaviour", or "Intermediate Temperature Embrittlement" (ITE).

One of the first systematic investigations of the influence of strain rate and temperature on the tensile ductility of copper-based alloys (namely OFHC – Oxygen-Free High Conductivity - copper and 70-30 α-brass) can be found in the early work of Greenwood[4]. Here, only one-half of the ductility trough was displayed, because the maximum testing temperature was 600°C. Figure 1 gives examples of full ductility troughs found with OFHC copper tested in tension under roughly similar experimental conditions, pooling data from several investigations. As seen, with the wider range of temperatures explored here, the curve takes indeed the shape of a trough, its value decreasing before rising past a more or less well-defined minimum. Note that the lower-temperature portion of the curve is roughly the same in all these studies of OFHC copper while the second, rising, portion differs significantly from one study to the other.

Figure 2a sketches main phenomenological features of the ITE phenomenon, showing the ductility trough (Domain II). Fracture within the trough is always intergranular. Several studies were conducted on single crystals in order to verify that grain boundaries are needed for the ductility trough to appear: copper single crystals are documented to rupture after deforming extensively to a knife-edge fracture surface between room temperature and 500°C in Ref.[5] or 450°C in Ref.[6]. Similarly, no ductility trough was observed for α-brass single crystals at intermediate temperature[5, 7].

The intermediate temperature embrittlement of copper and its alloys has its origin in the onset of creep[8]. It is associated with grain boundary voiding above a certain temperature range; for simplicity we shall designate hereafter this temperature range by means of a single lower-shelf temperature value, T_E, as sketched in Fig. 2a. As the temperature increases past T_E, there is a change in fracture path from transgranular to intergranular. As mentioned above, T_E is typically around 300 °C; however, it varies with the material and with test conditions such as the strain rate

or also the sample shape. Often, a temperature can be found where, for the alloy and testing conditions in question, the ductility passes through a minimum; this is typically around half of the metal or alloy melting point in Kelvin (roughly 400°C for pure copper, see Fig. 1).

The embrittlement often ceases at temperatures above another temperature range, which we shall again designate for simplicity using a single temperature, T_R. Typically, above T_R grain boundary mobility, often accompanied by dynamic recrystallisation, becomes operative. This restores ductility[2, 6, 9-13], as is often observed in metals and alloys[14, 15].

Corresponding tensile curve shapes are drawn in Fig. 2b. The sketch depicts the sharp decrease in ductility that is observed when testing above T_E and also the increased ductility in Domain III coupled with the characteristic tensile curve oscillations that often betray the presence of dynamic recrystallisation. Figures 2c and 2d show typical fracture surfaces, illustrating the transition in OFHC copper from transgranular fracture along the lower shelf to intergranular fracture in the trough. Figure 2e shows how the trough is visually evident on tensile tested bars.

Such behaviour exists in other metal systems; in particular, many of its features have parallels in steel. It has for example been demonstrated for steel that those variables which influence the shape (depth and width) of the ductility trough are also responsible for transverse cracking during straightening operations[16]. Compared with copper, the phenomenon is however more complex in steel, given the added presence of allotropic transformations in iron.

The intermediate temperature embrittlement of copper and its alloys has numerous consequences in industrial practice. One is that the deformation processing of copper and its alloys is typically carried out either at room temperature (using intermediate annealing steps to undo the effects of work-hardening) or alternatively at high temperature, often above 700°C, in order to avoid the critical range of intermediate temperatures. This is illustrated by the distinction sometimes made between “cold-working brasses” (α brasses, formed cold because they tend to be hot-short) and “hot-working brasses” ($\alpha+\beta$ brasses, formed hot because β and β’ are brittle at lower temperatures)[17-24]. The phenomenon obviously also plays an important role in the elevated temperature performance of copper and its alloys, and hence in their selection for engineering service[25].

Other practical consequences of the phenomenon are less obvious but can be quite important to industrial practice. Intermediate temperature embrittlement may prohibit the use of certain deformation processes. It can also cause cracking after deformation, as a result either of internal residual stresses or of transient thermal stresses during rapid temperature excursions. Such cracking in deformation processing is generally termed «hot shortness», or more accurately for

copper, « warm shortness». Engineering-oriented reviews dealing with the problems encountered during hot working of copper alloys can be found in Refs.[21, 24, 26, 27].

Related cracking phenomena in copper alloys can also be seen during casting[28] (as certain forms of hot tearing), extrusion[29], homogenisation[30], annealing[8, 31-33] (where it is termed "fire-cracking", *e.g.* for lead-bearing nickel silvers), or welding[34, 35]. An illustrated review[36] presents failures occurring on brass rods both during processing stages (casting, extrusion and cold-drawing) and during service (including environmentally induced failures – not treated hereafter – but also failure during secondary cold- and hot-deformation operations such as hot stamping or hot forging); its author additionally suggests corresponding corrective actions. Figure 3 gives two illustrations of cracks caused during processing by the intermediate temperature embrittlement of copper-nickel alloys. Hot ductility tests have also been used to quantify the intermediate temperature embrittlement phenomenon: deformation processing and elevated temperature usage can then be rationalised into processing maps designed as guides in forming operations[13, 37-48].

This article is a review of research on the intermediate temperature embrittlement of copper and its alloys. Its main goal is to present in a single venue the significant, but somewhat disparate, body of work on the phenomenon, while at the same time attempting to place it in the context of well-known elevated temperature failure mechanisms and embrittlement phenomena known to be active more generally in metals and alloys.

A simple general view of the link between the phenomenon and basic fracture mechanisms at high temperature is presented first, so as to expose the physical origin of the phenomenon and give meaning to its characteristic temperatures, T_E and T_R. We start with pure copper and then cover alloys. Next, focus is placed on two fundamental mechanisms that are known to enhance significantly the intermediate temperature embrittlement of copper and its alloys, namely grain boundary embrittlement and metal-induced embrittlement. These are reviewed in turn, focusing on aspects that are pertinent to copper. As variations in the results from one reference to another (see Fig. 1) can be imputed to differences in many experimental parameters, including for example grain size, metal purity, strain rate or test atmosphere, the influence of these parameters on the intermediate temperature embrittlement of copper and its alloys will also be illustrated and discussed throughout the article in each of its sections. We have aimed to provide relatively extensive coverage of the subject; however, given the amount of work that has been done, over many years, on copper and its alloys the article cannot be comprehensive. For example, the intermediate temperature embrittlement of irradiated copper materials[49-52] is not covered.

The ductility trough of unalloyed copper

Basic fracture mechanisms for face-centred cubic metals in general and for OFHC copper in particular have been reviewed based on an extensive compilation of experimental data, and summarised in the form of a fracture mechanism map by Ashby and co-workers[14, 53-55]. The fracture mechanism map proposed in Ref.[14] for OFHC copper is drawn in Fig. 4a in (dimensional) tensile stress / temperature space. As seen, all four mechanisms characteristic of face-centred cubic metals are operative in pure copper. At low temperature ($< 0.35\ T_M \approx 180°C$) copper fails by classical ductile fracture. In tensile testing of round bars, this is manifest by classical cup and cone fracture preceded by necking, the onset of which is well predicted by the Considere criterion, Fig. 2b. Above roughly 200°C, copper creeps (Fig. 4b) and rupture of the metal can be caused by several creep failure mechanisms (Fig. 4a). Transgranular creep fracture is characterised by ductile voiding and tearing within grains; since the material is essentially damaged everywhere and elongates extensively before fracture, this is generally not a brittle form of fracture. The second main mode of creep fracture, namely intergranular fracture, is characterised by voiding and fracture along grain boundaries. Since damage is then highly localised, this is a brittle fracture mode, characterised by a much lower global sample elongation at fracture, Fig. 2. In this domain, fracture occurs by grain boundary voiding, also called intergranular cavitation, Fig. 4a. This is characterised by a relatively flat fracture surface, generally accompanied by internal damage elsewhere within the material. At the highest temperatures and for high strain rates, tensile rupture is observed concomitant with dynamic recrystallisation. This is generally a ductile failure mode ending in tensile testing with tearing of the bar to a ridge or a point, Fig. 2e.

At the simplest level of analysis, since intergranular fracture is the only brittle failure mode on the map and since failure in the trough is indeed always intergranular, a one-to-one association can be proposed between intermediate temperature embrittlement and the region of intergranular creep fracture on the fracture mechanism map. Grain boundary voiding is typically described by two consecutive stages, namely (i) cavity (or void) nucleation and (ii) cavity (or void) growth. These have been addressed in detail by several authors; reviews are given in Refs.[56-59]. Cavity nucleation can be governed by three mechanisms, namely diffusion-driven vacancy accumulation, stress relief at the head of dislocation pile-ups, and grain boundary sliding at a non-planar grain boundary or a triple line. Cavity growth can also be governed by several rate-limiting processes. These include diffusion along grain-boundaries, diffusion along pore surfaces, creep deformation of material around the void, or combinations of these. These mechanisms can control the rate of void growth both locally (where damage progresses), and also more globally

when load transfer from damaging to non-damaging regions of the material dictates the local stress in damaging regions[56, 59]. In diffusion control, voids are either (i) rounded when surface diffusion is sufficiently rapid to equilibrate capillary forces ("r-cavities", typical of lower stresses in the field on the fracture mechanism map), or (ii) cusped or wedge-shaped ("w-cavities" seen at higher stresses) when surface diffusion is slow.

Intergranular cavitation has been documented in creep testing of both OFHC copper bicrystals[60-62] and commercial polycrystalline copper[63-65]. Grain boundary sliding has been shown to play a strong role in the voiding process: grain boundary irregularities such as bends or ledges, and triple lines at three-grain junctions or precipitates, provide sites of eased void cavitation along sliding boundaries[60]. A review of grain boundary sliding data in copper at intermediate temperature is given in Ref.[63], which also presents a phenomenological model based on consideration of stress concentrations created at the intersection of the primary glide plane with grain boundaries. The formation of intergranular cavities in copper at high temperatures has also been attributed to the pile-up of grain boundary dislocations[66-68]. Raj and Ashby propose a detailed analysis of the relationship between nucleation and growth of voids along grain boundaries and mechanical properties at elevated temperatures in Ref.[69].

The different hypotheses that have been proposed to model both the nucleation and the growth of voids and the possible influence of grain boundary sliding generally arrive at the prediction that there is a minimum time (and hence strain) to rupture at approximately half of the melting point when a polycrystal is deformed at a constant strain-rate[69]; this is indeed observed with copper (Fig. 1). This minimum arises from the interplay of void nucleation and void growth rates, the former being higher at lower temperature (because the flow stress is higher), while the latter dominates at higher temperature (because diffusion rates are higher). Since the rate of damage accumulation, and hence the inverse of fracture time, are proportional to the product of the void nucleation rate by the growth rate, the rate of damage exhibits a maximum, and hence the time to fracture a minimum, at some intermediate temperature near one-half the melting point.

Dynamic recrystallisation is observed in copper above around 700°C ($\approx 0.7\ T_M$); however, the precise value of the temperature at which it dominates depends on deformation conditions, as seen on the fracture mechanism map, Fig. 4a. In dynamic recrystallisation, a rapid accumulation of stored energy of cold-work, coupled with thermal activation, drives the nucleation and growth of new grains within the material while it deforms. As in static annealing, dynamic recrystallisation competes with dynamic recovery. Copper has a moderate stacking-fault energy, which slows recovery by inhibiting cross-slip. Hence, it is expected to be somewhat more prone to dynamic recrystallisation than higher stacking-fault energy face-centred cubic metals such as

aluminium or nickel; this is visible if one compares fracture mechanism maps of Ref.[14] at low dimensionless stress. The nucleation of new dislocation-free grains occurs preferentially at, or near, grain boundaries (often bulged and/or serrated by strain). Therefore, dynamic recrystallisation is more rapid in polycrystals, since these contain both grain boundaries and triple junctions, than in bicrystals and, even more so, than in monocrystals. This said, dynamic recrystallisation has also been reported for single-crystalline copper, where new grains are nucleated at deformation bands, twins or inclusions[70].

Typical stress-strain curves for deformation with dynamic recrystallisation are sketched in Fig. 5. Depending on the initial grain size, the temperature and the strain rate, flow curves can present either a single peak (corresponding to the initiation of grain nucleation and refinement) or multiple peaks (leading to grain coarsening)[70]. The dynamic recrystallisation of copper has been the object of numerous studies, using monocrystals[71-75], bicrystals[76-78], tricrystals[79-81] and polycrystals[38, 73, 82-98]. These all confirm the influences sketched in Fig. 5 of (i) strain rate[38, 73, 77, 83, 89, 92, 93, 96, 97], (ii) temperature[38, 73, 83, 87, 89, 92, 96, 97] and (iii) initial grain size[87] on the shape of the flow curves.

Dynamic recrystallisation, obviously associated with a certain mobility of grain boundaries, hinders grain boundary void growth; this in turn prevents intergranular fracture. The onset of dynamic recrystallisation therefore defines the upper shelf of the ductility trough; this is also observed in many other metals: steel, NiAl, nickel and FeNi are examples[16, 99-102]. The role of dynamic recrystallisation in tensile fracture being defined by competition with another mechanism, namely intergranular cavitation, the upper shelf transition temperature T_R is a function of parameters that affect either of the two mechanisms.

Looking at the fracture mechanism map of Fig. 4a, it appears that creep testing will not reveal the ductility trough. In a series of creep tests conducted either at fixed temperature and variable stress, or alternatively at fixed stress and variable temperature, only one transition is seen (such tests run along vertical or horizontal lines in Fig. 4a). Both sides of the trough are on the other hand apparent in constant strain-rate tensile testing. At a simplified level of analysis, the trough can be sketched on a fracture mechanism map by assimilation of a constant strain-rate tensile test with a creep test that displays the same imposed strain rate as its secondary stage ("steady-state" or minimum) creep rate. This is of course somewhat crude, but since the creep of copper has been the object of numerous studies focused on the steady-state creep regime (*e.g.*, Refs.[64, 65, 103-119]), and since this simple view of the ITE phenomenon illustrates well both its origin and its intrinsic dependence on several parameters, we adopt it here.

The deformation mechanism map of Ashby and co-workers for OFHC copper[120] is plotted, after conversion to dimensional tensile stress and temperature axes, in Fig. 4b. If we now superimpose constant strain-rate curves of Fig. 4b over the fracture mechanism map in Fig. 4a, we obtain the graph in Fig. 4c. Note that, within the intergranular fracture mechanism domain, these curves run broadly speaking parallel to lines of constant time to rupture drawn on the fracture mechanism map of Ashby et al. (Fig. 17 of Ref.[14]), showing that within this region of the map, the Monkman-Grant relation is roughly valid[121]. A few tensile test data for OFHC copper with a grain size near (in fact somewhat below) 100 μm are also plotted on Fig. 4c: as seen, the agreement with the curves is relatively good, in terms both of fracture mode and strain rate.

The ductility trough then becomes visible as that portion of the lines along which they traverse the region of intergranular fracture. The lines cross into this region from regions of ductile fracture through transgranular fracture at low temperature, and leave it at its upper shelf by entry into the region of dynamic recrystallisation; these features correspond indeed to general characteristics of the intermediate temperature embrittlement of copper and its alloys.

This simplified view of the ductility trough phenomenon additionally explains why it is essentially absent in some metals, such as aluminium. Indeed, in pure aluminium, the intergranular fracture domain is altogether absent[14]. In commercial purity aluminium, such a region exists[14]; however, creep data are such that constant strain-rate curves generally do not cross into this region, running instead roughly parallel to the boundary that denotes the transition from one to the other of the two fracture mechanisms[122, 123].

Influence of strain rate

The dependence of the phenomenon on strain-rate is then immediately apparent: the higher the strain rate, the higher the line through the graph (Fig. 4c) and thus the narrower the trough, as was already sketched by Wray in 1969[124]. This is indeed observed: except for very rapid (impact) deformation, as the strain rate increases the ductility trough of pure copper narrows and becomes more shallow[6, 9, 13, 90, 125-131]. Figure 6 illustrates this for pure copper using data from several sources[6, 127, 129]: the higher the strain rate, the narrower and the shallower the trough. At the highest rates (above 1 to 10 s^{-1}) the trough disappears altogether. Figure 7 gives a cross-section near the fracture surface of a sample of OFHC copper tested in tension under the same conditions at two strain rates (from Ref.[129]). At the lower strain rate (right-hand micrograph), there is extensive intergranular damage accumulation within the material, whereas at the higher strain rate (left-hand micrograph) there is essentially none: the transition in fracture mode is quite apparent.

Influence of grain size

The influence of grain size is less obvious than that of the strain rate; however, this too can be discussed using Fig. 4. An increase in grain size will obviously deepen the trough somewhat. Indeed, the strain to failure will then decrease since the fraction of (shearing and dilating) grain boundary region material will be smaller in relation to the remaining material[13] thus lowering the sample elongation upon intergranular fracture; this can be seen in the data of Fig. 6.

The influence on trough width is more complex. As the grain size is varied, fracture mechanism maps should not change greatly as long as the (areal) density of void nucleation sites along grain boundaries does not depend on grain size; this will for example be when intergranular voids nucleate at the intersections of grain boundaries with slip planes, or at grain boundary inclusions and precipitates. If, on the other hand, voids nucleate mainly on grain boundary triple lines, finer grains will nucleate more intergranular voids, thus expanding the range of dominance of intergranular fracture and hence the trough width. A priori, this effect should at least become noticeable at grain sizes so small that triple lines become more frequent than other intergranular void nucleation sites.

Now, the creep rate of copper depends only weakly on grain size at higher stress, both in the power-law (dislocational) creep regime (where $n \approx 5$) and near the transition to the regime where $n \approx 1$[132]. On the other hand when $n \approx 1$ (generally but not always taken to be the diffusion creep regime), the creep rate depends roughly on the inverse of the grain size squared[111, 113, 133]. The range of dominance of this latter (diffusion creep) regime is sketched in Fig. 4d for various grain sizes: as seen, when the grain size falls below 10 μm diffusive creep will start being observed only at very low strain rates (below roughly 10^{-6} s^{-1}) while it will dominate at higher strain rates when grain diameters approach one micrometer. An increase in grain size should thus not affect the trough width much when grains are roughly above a few micrometers. For grains smaller than this, increasing the grain size should narrow the trough, because (i) if diffusion creep obtains, then the flow stress at given strain rate will be higher, causing stress-temperature iso-strain-rate curves to shift upwards and cross a narrower portion of the upper right-hand corner of the intergranular creep fracture region, and/or because (ii) an increase in grain size causes, if anything, a reduction in void growth rate (since the triple line density decreases) causing in turn a reduction in the range of dominance of intergranular fracture.

Data for copper from hot tensile tests show that the greater the grain size, the deeper the ductility trough becomes (except in one instance at the smallest grain sizes), while the influence

of grain size on trough width is not very clear[107, 127, 134]. As the data are for grains greater than 10 μm, these trends are overall as expected.

Influence of prior cold work

Data for copper also show that room-temperature prestraining of the pure metal sufficient to suppress plastic deformation upon loading in creep testing within the range of dislocation creep and intergranular fracture does not affect grain boundary damage significantly; however, this lowers the strain rate of the grain interiors, and hence of the metal[113, 114, 116]. These results suggest that prior cold-working of the metal (i) should lower the tensile elongation at failure in creep (constant load) deformation, and (ii) should deepen and narrow the trough under fixed strain-rate deformation. Indeed, if prior cold-work does not affect grain boundary damage significantly, it will leave the fracture mechanism map boundaries relatively unaffected. Given that cold-work will on the other hand raise the flow stress and hence if anything shift iso-strain-rate curves upwards in Fig. 4c, it will narrow the intersection between these curves and the region of dominance of intergranular fracture.

Influence of alloying

Solid solution hardening

Alloying as a rule suppresses neither intermediate temperature embrittlement nor intergranular cavitation; data exemplifying this can be found for brass tested in tension at intermediate temperature in Refs.[4, 20, 135-137] or for other copper alloys in Ref.[8]. On the other hand, while it does not suppress the phenomenon, alloying influences it[138].

The four alloying elements that are used at elevated concentrations in copper, namely Zn, Sn, Al and Ni, affect bonding, diffusion and sliding at grain boundaries. These alloying additions therefore influence mechanisms of intergranular failure, as well as the flow stress and the character of dislocational slip, notably because their presence alters the stacking-fault energy. This last parameter is important, as it alters both the character of slip and the rate of recovery, affecting in turn both the flow stress and the rate of damage accumulation in the deforming material. Gallagher and Murr have compiled data for the influence of alloying additions on the stacking fault energy in copper alloys; see Fig. 6 of Ref.[139] and Table 3.9 of Ref.[140]. A lowered stacking fault energy will tend to concentrate slip in defined glide planes, thus encouraging void nucleation as well as (plasticity-driven) void growth along grain boundaries. This will also reduce the rate of recovery, and in turn increase the flow stress at given strain rate in tensile tests, or lower the creep rate at given stress in creep tests[141]. Figure 8 shows the reduction in normalised

creep rate that results from changes in the normalised stacking fault energy in α-brasses (redrawn from Mohamed and Langdon[142]).

The influence of zinc content on the intermediate temperature embrittlement of brass was measured in Refs.[126, 143]. Data show that small additions of zinc have a beneficial effect on the hot ductility of copper whereas further additions are deleterious; this is illustrated in Fig. 9. Both grain boundary sliding and grain boundary migration are known to be significantly reduced by adding zinc. Also, the known decrease in stacking fault energy with increasing zinc content (Fig. 8) favours planar slip, encouraging the formation of dislocation pile-ups at grain boundaries[143]. The improvement in ductility with low additions of zinc (< 5%wt.) is thus attributed to a reduction in grain boundary sliding. The reduction in ductility that follows with further zinc additions is attributed to an increased rate of void nucleation and growth along grain boundaries intersected by coarse slip bands[143]. Note, however, that these trends also depend on extraneous factors, such as the respective purities of the metal and the alloy being compared (see below).

The creep behaviour of tricrystal and bicrystal specimens of Cu-9at.%Al between 500°C and 800°C was investigated in Ref.[144]. It appears from this study that a triple line either lowers the rate of grain boundary sliding until 650°C and consequently delays intergranular fracture, or alternatively promotes crack nucleation at temperatures higher than this[144].

In tin bronze, a study shows a significant decrease (by more than 100°C) of T_E upon adding 6wt.% tin to copper[145]. This deleterious influence can be explained either (i) by a promotion of localised slip and stress concentration at grain boundaries caused by the ensuing reduction in stacking fault energy[139] or (ii) as a result of grain boundary enrichment with tin causing a decrease in grain boundary cohesive strength[145].

In cupronickels, increasing the nickel content from 6wt.% to 30wt.% progressively decreases the intermediate temperature tensile elongation from 40% to 10%, this decrease being associated with an increase in the intergranular character of the fracture surface. These observations were related to a delay in dynamic recrystallisation at higher nickel concentrations[146]. Reid and Greenwood[9], on the other hand, found that alloying OFHC copper with nickel in the concentration range from 0 to 40wt.% reduces the trough, making it both narrower and shallower. It is interesting to note in connection with cupronickel behaviour that an embedded atom method simulation of grain boundary composition in Cu-Ni alloys predicts strong segregation of copper to both grain boundaries and free surfaces; hence, whereas copper is predicted to embrittle nickel alloys, this is a priori not expected of nickel in copper[147].

These are the trends that can be deduced to result from alloying; however, it is important to note that other parameters also influence the intermediate temperature embrittlement of copper and its alloys (purity, grain size and strain rate), and that their values vary from study to study. Therefore, although there are many studies of intermediate temperature embrittlement in monophase copper alloys (*e.g.*, Refs.[128, 148-150]), it is difficult to confront results across such studies to arrive at general statements concerning the influence of alloying additions.

Multiphase alloys

Dispersion-hardened copper alloys are generally used when high temperature strength is desired. At elevated temperatures, dispersoids act in large part to hinder grain boundary sliding (the presence of which was nicely evidenced using oxygen-containing Cu-0.065wt.%B bicrystals, where grain boundary sliding was visualised through the shear deformation of intergranular liquid B_2O_3 particles[151]). Solid particles resist such shear and thus hinder grain boundary sliding.

Intermediate temperature embrittlement has been characterised in copper containing dispersed particles of Al_2O_3 [6, 152], GeO_2 [153, 154] or SiO_2 [155-160]. In Cu-GeO_2 polycrystals it was also confirmed that the initial decrease in ductility occurs indeed with the onset of grain boundary sliding[153]. Since grain boundary particles hinder grain boundary sliding, their presence should retard the onset of creep fracture. In this sense, particles should be beneficial, as they can retard intergranular creep fracture and increase the lower shelf temperature T_E.

On the other hand, particles also act as preferential sites for the nucleation of voids because they concentrate stress in their neighbourhood[153, 155, 156, 161]. Finite-element calculations in Ref.[160] visualise stress distribution around such particles, showing that these depend strongly on the particle shape. For this reason, particles can accelerate creep fracture, both intragranular and intergranular; Fig. 10 illustrates this for internally oxidised Cu-Al [6]. This, in turn, will lower T_E if it is defined as that temperature where the ductility falls below a given value[153, 156].

Regarding T_R, particles retard recrystallisation and grain boundary motion[6, 13, 153, 155, 156]; however, the effect depends on the size and distribution of the particles[155, 162]. Two opposing effects have (again) to be considered: (i) the stress concentration created near the particles is a driving force for recrystallisation but (ii) the mobility of grain boundaries is reduced because they are pinned by particles[13, 163]. Ductility recovery has also been associated with diffusion-driven stress relaxation along copper-particle interfaces[157, 159]. With an increase in particle volume fraction, the ductility trough thus becomes narrower and sharper in Cu-SiO_2 [157, 159]. On the other hand, the trough is both deepened and widened in internally oxidised Cu-0.1wt.%Al, Fig. 10 after

Ref.[6]; the influence on the upper shelf is attributed to the fact that alumina dispersoids pin grain boundaries and hence hinder recrystallisation.

Concerning the effect of the size of the particles, data show that small particles ease void formation (as observed in steel[16]) but also ease diffusional stress relaxation[156], while bigger particles seem more effective in increasing the ductility by suppressing more strongly grain boundary sliding[154]. Changes in void nucleation mechanism, and hence in ductility, may thus be seen in dispersion-hardened copper as the size of the particles is altered[154]: grain boundary sliding-induced void nucleation at copper-particle interfaces is observed for small particles, while grain boundary sliding-induced void nucleation between particles (in the particle-free areas along the grain boundary) is seen with larger particles. Refining second phase particles, all else being constant, should also widen the trough by increasing T_R, since finer particles are more efficient at pinning grain boundaries (as the Zener relation shows).

With higher volume fractions of second phase, no simple trends can be proposed because the alloy behaviour depends on that of the other phase in addition to the copper-based α-phase. In brass, the body centred cubic β phase tends to see its ductility increase with increasing temperature. Therefore, multiphase $\alpha+\beta$ alloys can actually display what amounts to a ductility "hill" at elevated temperature (Fig. 11 of Ref.[13]).

We finally note that in some high-strength copper alloys intergranular fracture may be observed, not as a result of intergranular voiding, but rather because grain boundaries are lined with a brittle second phase. Ductility trough behaviour is then not generally observed (higher flow stresses, and hence lower temperatures, being more likely to crack brittle particles); however, temperature and thermal history exert an influence on the ductility of these alloys via their influence on factors such as grain boundary precipitation or elastic anisotropy. An example is given by Cu-14%wt.Al-Ni shape-memory alloys. In these alloys intergranular fracture is promoted by a high elastic anisotropy, and is also influenced by the various (brittle or ductile) second phases that can line grain boundaries[164-169].

Influence of strain rate and grain size

As for pure copper[6, 9, 90, 125-129] and except for very rapid (impact) deformation, as the strain rate increases the trough narrows and becomes more shallow for brasses[68, 125, 126, 128, 137, 143, 150, 170-173], bronzes[174, 175], cupro-nickel alloys[9, 176-178] and dispersion hardened copper[6, 153, 160, 179, 180]. For two (70-30 and 80-20) α-brasses, T_E was found to be strain-rate dependent, but not T_R [171]. Provided fracture mechanism maps are not fundamentally changed by alloying, this dependence on strain

rate conforms with the simplified description of the trough proposed for pure copper. Also consistent with this description is the lesser dependence of T_R on strain rate, given the nearly vertical orientation of the line delineating the onset of dynamic recrystallisation on the fracture mechanism map, Fig. 4a. The recorded ductility trough also increases in width and depth as the alloy grain size increases for brasses[8, 143, 150, 170-173, 181, 182], bronzes[3, 174, 175] (Fig. 11), and cupro-nickel alloys[176, 177, 183, 184].

Influence of purity and grain boundary embrittlement

Although a few general trends can be drawn from data concerning the influence of basic microstructural parameters, these are often not very clear; an example was given above for the influence of grain size on the ITE of nominally pure copper. One main reason for this is that the intermediate temperature embrittlement of copper is also strongly influenced by certain specific alloying additions, even when these are present only at very small concentrations.

In pure copper, the trough depends on how "pure" the copper is; see the lowest plot in Fig. 6. This is also illustrated in Fig. 12, which presents the ductility troughs observed for roughly similar (low) strain rates in different varieties of "pure" copper, ranging from oxygen-free copper (Cu OFHC) to 99.999999% pure copper (Cu 8N). As seen, the width and depth of the trough varies quite strongly indeed. It is essentially suppressed (at testing conditions of these data; changing the strain rate or the grain size may cause it to reappear) for 8N copper[185] whereas it is particularly well-defined for the oxygen-free copper (Cu OFHC)[186]. There are several reasons for this. One is quite obvious, namely the fact that the onset of dynamic recrystallisation, marking the extent of the upper shelf region, depends on the mobility of grain boundaries, which can be dramatically reduced by even small quantities of certain solute elements[92, 187].

The strong dependence on minor impurities of the ductility trough behaviour of copper is, in fact, one of its most salient - and complex - characteristics. The ductility trough behaviour experienced by copper and its alloys is thus to be placed in the wider context of intergranular embrittlement phenomena observed with many metal alloys: we attempt to do so in the two next sections of the review.

First, we review here the phenomenon from the viewpoint of classical embrittlement: impurities, even at small concentrations, can segregate to grain boundaries and modify these extensively, even at very small overall concentrations. Segregated impurities can alter the grain boundary bond strength and can also change the grain boundary diffusivity. In both cases minor additions can influence strongly the intergranular fracture of alloys. In this more classical form of

embrittlement the embrittling species has segregated before fracture, and by changing the grain boundary composition it changes the rate and level of damage and failure at grain boundaries.

Then, in the next section of this review, we turn to dynamic forms of embrittlement. Indeed, impurities or alloying additions can also interact dynamically with time-dependent failure processes, either by stress-induced diffusion to sites where these facilitate fracture, or because these take the form of a liquid that can rapidly flow along with the tip of a moving crack.

Grain boundary embrittlement

If ductility trough behaviour is documented even for pure copper[185, 186], the phenomenon can as mentioned be stronger in commercial copper and its alloys. It is amplified by the segregation, prior to fracture, of certain specific atomic species to grain boundaries: this general phenomenon, called "grain boundary embrittlement", is documented in many other systems, including alloys of iron or nickel, *e.g.*, Refs.[16, 188-199].

Grain boundary embrittlement has been amply documented for copper and its alloys; classical examples of embrittling elements are bismuth and antimony[196]. The ratio between grain boundary and bulk concentration can reach 10^3 to 10^5 for impurities having low solubilities: the width of grain boundary segregation layers being typically on the order of a few atoms only, even very small bulk concentrations of impurity atoms can then lead to significant concentrations of these atoms at a grain boundary. Minute embrittler concentrations, of a few tens of ppm, therefore suffice to enlarge the ductility trough of copper; Fig. 12 illustrates this. Because segregation is driven by enthalpy reduction and opposed by entropic effects, it becomes more pronounced at lower temperatures and can disappear altogether above a certain temperature (the thermodynamics of interfacial and grain boundary segregation are covered in Refs.[190, 194, 196, 199-205]).

There is a dependence of the embrittlement phenomenon on the prior time-temperature history of the material: this is simply related to the need for the embrittling species to migrate to the grain boundary or other site of fracture initiation for it to have an effect[8, 199, 203, 206-211]. Because decreasing temperature tends to increase the segregation driving force and decrease the segregation rate (which is generally limited by the rate of diffusion of atoms, either in the bulk or along grain boundaries), segregation effects are most visible in a certain intermediate range of temperatures. It was thus found in one semi-quantitative study of copper-nickel-tin alloys that impurity-associated embrittlement can result from prior exposure to temperatures above the temperature of tensile testing: the dependence of embrittlement on annealing time and temperature showed the classical «nose» shape on a TTT diagram[8]. The fact that segregation and

embrittlement are most extensive in roughly the same range of "warm" temperatures of copper deformation processing is of course one reason why segregation amplifies so markedly the intermediate temperature embrittlement of copper and its alloys.

Segregation can embrittle metal alloys at intermediate temperatures in several ways. Minor additions of segregating species can lower the alloy surface energy. As a result, this aids the nucleation and growth of cavities. Impurities can also modify grain boundary diffusivity, in turn reducing the rate of relaxation of stress concentrations along grain boundaries[188]. Segregation can modify the interatomic cohesion of atoms, both solvent and impurity, along both grain boundaries and free surfaces. This phenomenon is very complex (*e.g.*, Refs.[194, 212, 213]), such that neither qualitative nor quantitative effects of segregation on the intrinsic strength or fracture energy of grain boundaries are fully predictable at present. An example can be found in the copper–bismuth system where both atomic size effects[214, 215] and electronic effects[216] are said to be responsible for the strong bismuth-induced embrittlement of copper grain boundaries.

A few interesting rules have nevertheless been proposed in the literature, allowing some degree of predictability of the potential effect of segregation on grain boundary cohesion. These are usually focused on the intergranular embrittlement of iron but governing principles are generally transposable to copper.

Seah proposed a now well-established theory based on the regular solution model according to which segregation will occur if the sublimation enthalpy of the segregant is lower than that of the "solvent" matrix metal[196]. Figure 13 presents the results obtained in Ref.[196] from thermodynamic data. The position of copper is highlighted (using full symbols) together with that of its stronger embrittlers: it is clear that this simple criterion works well for all of these well-known embrittlers - as it also does for iron and steel. On the basis of an analysis of the physics of grain boundary fracture, embrittlement is predicted by Rice and Wang[194] to occur if the surface segregation free energy is higher (in absolute value) than the grain boundary segregation free energy (evaluated in the dilute limit and by neglecting secondary terms): elements that segregate more strongly to free surfaces than to grain boundaries weaken grain boundaries. A recent study of the copper–bismuth system supports such a criterion[217] as does an older study of copper–antimony[218]. In brief, confrontation of these two criteria with data shows that these represent necessary conditions, in that these criteria are indeed fulfilled by elements that cause grain boundary embrittlement. More work is needed to ascertain whether this is always true and whether these are also sufficient conditions for embrittlement[217].

There might indeed be other necessary conditions. If dislocation emission at the tip of a crack, causing in turn crack blunting, requires a lower stress than is necessary to cause crack

propagation, it may mask the influence of segregation on the local energy of grain boundary fracture, $2\gamma_{int}$ [194]. Atomistics of the fracture process are also more complex than can be accounted for by macroscopic chemical thermodynamics, a fact that Rice and Wang pointed out[194]. The complexity of processes that govern multicomponent grain boundary separation is for instance evidenced by the fact that, when impurity atoms X segregate to grain boundaries in, say, copper their presence will not only introduce two new bond types (X-X and Cu-X), but may also, by charge transfer, alter the strength of Cu-Cu bonds in the neighbourhood of the boundary. This is for example suggested by evidence for asymmetric segregant distributions across both sides of fractured grain boundaries in some systems, an observation that can be explained if the crack path was near, but not at, the segregant-rich grain boundary[219].

The embrittlement of copper

Embrittling elements are many in copper alloys. These include: Bi [10, 21, 146, 214, 216, 220-243], Te [10, 21, 244, 245], S [10, 21, 106, 130, 143, 178, 186, 246-250], Sn [11, 21, 200, 206, 208], O [109, 158, 209, 251, 252], Sb [21, 200, 218, 233, 251, 253-258], Pb [10, 21, 259] and Se [10, 21, 245] as well as C and, in some but not all instances, P [21, 145, 174]. Gavin ranks their potency in the order of (most to least potent) Bi, Te, Pb, Se, S [10]. Putting together data from the literature, the ductility trough of copper and its alloys indeed widens both at its lower and at its upper limits (which respectively decrease and increase) and also deepens (*i.e.,* the measured ductility falls further) as the percentage of embrittling impurities named above increases[1, 2, 10, 11, 223, 259, 260].

More generally, metal grain boundary embrittling elements tend to belong to columns IV to VI of the periodic table[188, 192, 261]; this is indeed true of all elements mentioned in what precedes. Embrittling species also tend to be more electronegative than the host metal[192]. Figure 14 represents a partial view of the periodic table of elements where copper is highlighted together with the position of its stronger, well-established, embrittling segregants. Note that oxygen counts among embrittling species[109, 158, 209, 251, 252]. This has the important consequence that copper and its alloys can be embrittled by interaction with the atmosphere; evidence of this can be found in Fig. 4 of Ref.[118].

A reverse, "de-embrittling", effect is documented to result from the addition of certain elements, also noted to reduce the incidence of practical problems related to the ductility trough behaviour of copper: Zr [12, 249, 262-264], as well as Mg [146, 175], B [175, 186], Y [265-267], Ce [266], La [266], Ca[266], Nb [34], Li [268], U [264] and - but to a lesser extent - P [175] and Ti [12, 186]. Foulger reports that Mg and Li improve the ductility of cupronickels at 900°C [21]. A 1995 patent cites B and Mn as additions decreasing crack formation (in both casting and deformation) of nickel-containing copper

alloys[269]. Note that the elements Li, Mg, B, Y, Ce, La, and Ca all belong to Columns II and III of the periodic table, Fig. 14. The role of Zr, Y, Ce and La has been explained as being a result of their ability to scavenge sulphur[12, 175, 249, 265, 266].

A comparison with nickel alloys is interesting. In addition to the strongly detrimental element sulphur, in nickel the elements Se, Sn, Te, Tl, Pb, Bi are documented embrittlers, while the elements Ti, Zr, Hf, La, Y, Mg, B, Ca, Nd and Ce are documented to be beneficial additions[188]. The authors of Ref.[188] also mention that all these beneficial elements combine with sulphur in nickel.

Sulphur, a well-known culprit also in iron and nickel alloys[188], has often been named as responsible for the intermediate temperature embrittlement of many copper alloys, although the way in which sulphur segregation decreases mechanical properties of copper is not perfectly clear. Even at very low concentrations, sulphur can be well above its equilibrium solubility. The latter was theoretically investigated in Ref.[270], showing that the sulphur solubility in copper is limited mainly by the formation of a very stable intermediate phase, Cu_2S. Formation of this compound is rapid (because of the high mobility of sulphur-vacancy defect pairs) and it appears in selected segregation sites such as grain boundaries according to Ref.[270]. As a consequence, every other impurity that has attractive interactions with vacancies and/or segregates to copper grain boundaries and/or forms more stable sulphur components may be expected to improve the mechanical properties of copper alloys because it will compete with the grain boundary segregation of sulphur. Hence, the ambivalent action of P (positive in Ref.[175] and negative in Refs.[21, 145, 174]) may be put in parallel with that in steels where it reduces sulphur-induced embrittlement (being a segregation competitor) at higher (creep) temperatures, while it reduces grain boundary cohesion at low temperature, thus promoting brittle intergranular cleavage[188].

In the experimental study of segregation-induced intergranular fracture, Auger Electron Spectroscopy (AES) is a powerful technique because - provided adequate sample preparation is used, this generally involving *in-situ* sample fracture under high vacuum - it enables detailed analysis of only a few atomic layers along the surface of conducting material[195]. Descriptions of the technique can be found in Refs.[271, 272] and in the numerous and seminal publications of Seah et al.[273-275]. AES has thus frequently been used to characterise fracture surfaces of copper alloys[3, 12, 106, 145, 174, 222, 245, 247, 252, 255, 265, 266, 276], at times coupled with other surface analysis methods[277]. All these references document that, when copper and its alloys fracture by brittle intergranular fracture, grain boundaries are indeed generally decorated with a high concentration of embrittling species. Thus quantified concentrations of embrittlers are often correlated with models describing their intergranular segregation; these are essentially all based on the initial work of McLean[278].

Alternative techniques have also been developed in recent years to give access to grain boundary chemistry at atomic-level resolution. These include the atom probe and high-resolution analytical electron microscopy; a succinct review with references for further reading can be found in Ref.[279].

An important consequence of the role of grain boundary embrittling elements is that, in the range of grain sizes where grain boundaries are not fully saturated yet contain an appreciable fraction of the total embrittling impurity atom content, the larger the grain size is, the higher becomes the concentration of embrittling species along the grain boundaries, and hence the weaker the material becomes with regard to intergranular fracture. This fact helps explains why, in copper and its alloys, the ductility trough width often increases as the grain size increases[3, 8, 107, 127, 134, 143, 150, 170-177, 181-184], even though this is not expected based on simple reasoning (since neither grain boundary voiding nor creep rates in the range of stresses near the transition between intracrystalline and intercrystalline fracture, Fig. 4, -i.e. all of Fig 4- should be much affected by grain size, all else being constant; see above).

Influence of grain boundary character: grain boundary engineering

Many grain boundary phenomena that intervene in the intermediate temperature embrittlement of copper are related to the grain boundary structure and energy. These include grain boundary sliding (only random boundaries readily absorb lattice dislocations such that sliding is more difficult for special boundaries[280]), grain boundary mobility, grain boundary thermal stability, grain boundary diffusion (consequently intergranular cavitation) and grain boundary segregation (consequently grain boundary embrittlement). A recent overview by Watanabe[281] thus correlates the structure of the grain boundaries with their mechanical properties at high temperature.

Bicrystals have often been used to investigate the influence of grain boundary character on intergranular sliding rate[161] and fracture in copper and its alloys[62, 66, 68, 151, 155-158, 160, 171, 180, 258, 282-284]. Results show that grain boundary sliding rates are much lower for low-index (013) and (012) twins than for other more highly misoriented bicrystals disoriented by rotation around <011> [161]. Similarly, it was observed that boundaries close to an exact coincidence site lattice misorientation show little deformation activity during diffusional creep in polycrystalline samples of Cu-2wt%Ni [285]. Correlations can be made between fracture processes and the grain boundary energy, in which it appears clearly that random grain boundaries are more prone to intermediate temperature embrittlement than special boundaries[68, 151, 156, 157, 283, 284]. This can be related to both the intrinsic grain boundary cohesion, which is higher for special boundaries, and to segregation effects, which are lower for special boundaries given the lower energy released upon decoration with segregants[258].

This, in turn, implies that engineering the distribution of grain boundary character within polycrystalline copper and its alloys (a strategy for material improvement called "grain boundary engineering"), holds significant promise towards minimising intermediate temperature embrittlement, either directly (by modifying the proneness of grain boundaries to cavitation and fracture), or indirectly (by modifying the level of damage-mitigating constraint exerted by surrounding intact regions). Recent explorations of the grain boundary engineering of α-brass can be found in Refs.[286-290] and in Ref.[291] for α–β brass; the grain boundary engineering of pure copper is investigated in Refs.[292-297]. Extensive data show that it is possible, through selected thermomechanical treatments, to increase the proportion of CSL (coincidence site lattice) grain boundaries; however, no mechanical data pertinent to ductility trough behaviour could be gleaned.

Metal-induced embrittlement

In addition to grain boundary embrittlement, a second class of mechanisms can increase the severity of ductility trough behaviour in copper and its alloys; these are grouped under the denomination "metal-induced embrittlement" (MIE). This includes notably "liquid metal embrittlement" (LME), but also the slower mechanism of "solid metal embrittlement" (SME). The ductility trough behaviour and associated hot or warm shortness, of copper and its alloys have thus, in several practical instances, been attributed to liquid or solid metal embrittlement[298, 299], as has the fire-cracking phenomenon observed in nickel silvers (Cu-Ni-Zn alloys)[31-33].

Metal-induced embrittlement differs from grain boundary embrittlement in that the embrittling metal migrates *during* fracture to the site of crack nucleation and growth. Given its importance, the phenomenon has been extensively studied. Several theories have been proposed to explain liquid metal embrittlement, and by extension solid (and vapour) metal embrittlement; these are reviewed in Refs.[298-309].

In brief, none of the theories proposed to date provides a complete and predictive theory of the phenomenon. By and large, it nonetheless is recognised that, at the heart of MIE processes, is the fact that the embrittling metal reduces the strength of atomic bonds in the base metal, just as do solid state embrittling grain boundary segregants. This in turn leads to lowered capillary energy requirements for fracture, and should logically also ease local slip near crack tips, as suggested by Lynch[304].

MIE, and more specifically LME, vary strongly in severity with the material system at hand: this has been termed the «specificity» of MIE. Some common characteristics tend to be featured by documented embrittled/embrittler metal pairs: low mutual solubility, lack of mutual

intermetallics, similar electronegativity[298, 301, 302]; however, all rules that have been proposed so far suffer exceptions[302]. It is often stated that MIE is far more general than published data may imply, to the point where even the notion of any «specificity» of the phenomenon has been disputed, particularly for LME[302, 307, 310].

One main reason why the occurrence of MIE is judged wider than data suggest, is that observation of the phenomenon is highly dependent on testing conditions (temperature, strain rate, presence of a notch etc). An important cause for this dependence is the need, in the study of LME, for good wetting between the embrittling liquid and the solid metal, which is often difficult to produce with liquid metal[301, 302, 307]. Fracture by MIE is generally intergranular in polycrystalline materials[298, 299, 301, 302]; however, this is not always so and even single crystals or amorphous alloys are sensitive to the phenomenon (*e.g.*, Refs.[302, 304]).

Solid Metal Embrittlement

As stated above, grain boundary embrittlement is caused by the migration, before fracture, of impurity atoms from the bulk metal to grain boundaries, Fig. 15a. By changing the local composition and bond strength at the grain boundary, impurities lower the local grain boundary work of separation γ_{int}. If one neglects atomistic effects that have been reasoned to be of second order[194], then one may write:

$$\gamma_{int} = 2\,\gamma_{SV} - \gamma_{GB} \qquad \text{Eq. 1}$$

where γ_{SV} is the solid surface energy and γ_{GB} the grain boundary energy. Since impurity segregation will most often lower $2\,\gamma_{SV}$ significantly more than γ_{GB}, it will tend to favour fracture[194, 219].

Fracture is generally rapid in comparison with the rate of atom migration in the solid state. Therefore, in the absence of diffusion, the separated grain boundary surfaces generally see their total impurity content unchanged. At the simplest level of analysis, solute is then distributed equally along the fracture surface, such that its concentration there is one-half that along the grain boundary, Γ_o^s, Fig. 15b. In solid metal embrittlement, the situation is changed by the fact that fracture is sufficiently slow to allow diffusion of the embrittling species. If fracture is quasistatic, i.e., sufficiently slow for the embrittler concentration to attain full thermodynamic equilibrium (constant and uniform chemical potential μ) under the relevant sample testing conditions, the local work of fracture is changed in two respects.

First, the impurity concentration along the opening grain boundary and the newly formed free surfaces changes simultaneously with decohesion, to adjust for the difference in equilibrium

concentration at fixed chemical activity μ between grain boundaries and free surfaces, Fig. 15c [147, 194]. This will always lower the free energy of decohesion, γ_{int} [194]; hence, the embrittling effect of the segregant is amplified. In practice, since the actual free surface concentration will be intermediate between these two extremes, one has[193, 202]:

Eq. 2

Secondly, the equilibrium grain boundary segregant concentration may depend on the applied stress, particularly if the stress is high, as will be the case near the tip of a crack, Fig. 15d. Given time to diffuse, therefore, the embrittling species may (further) lower the grain boundary cohesion and drive crack propagation, ending in fracture (indeed, *a priori* one would expect species that lower the local modulus, and hence the local bond strength, to migrate to a stressed region). This phenomenon is called "dynamic embrittlement", defined as fracture resulting from the stress-induced diffusion of an embrittler to the tip of an intergranular crack, reducing the strength of the grain boundary and promoting intergranular fracture[130, 131, 208, 209, 263, 311-317]; see Ref.[318] for a recent review.

Segregant diffusion to newly created free surfaces and/or to stressed grain boundaries can thus create a time-dependence of grain boundary fracture, and hence of intermediate temperature embrittlement. The kinetics of impurity migration during fracture were analysed for slow separation (constant μ), fast separation (constant X_{gb}) and transient regimes in Ref.[319]. In essence, the dynamic embrittlement model considers a given stressed material A containing an intergranular crack and an embrittling species B that segregates to regions of high tensile stress concentration. Governing equations are written for (i) the grain boundary diffusion of B under the action of an applied stress gradient, giving the intergranular concentration profile for B along the grain boundary ahead of the crack tip as a function of time and (ii) the grain boundary cohesion (and hence intergranular rupture stress) of A as a function of the intergranular concentration of B. Comparison of the grain boundary cohesive stress with the stress field ahead of the crack tip then gives a criterion for, and the rate of, crack advance. All equations are treated in one dimension. A main difficulty in the analysis lies in the phenomenological assessment of the grain boundary cohesion of A as affected by the presence of diffusing B atoms. Numerical calculations lead to satisfactory agreement of the model with experimental observations (namely crack-growth rate) if and only if the stress-driven diffusion of B ahead of the crack tip spreads only within a nanometre-long crack-tip "cohesive zone" [320]. Crack-growth rates are found to be on the order of 1 μm/s for both Cu-Sn polycrystals[206] and Cu-Sn bicrystals[208]. Polycrystals show discontinuous propagation[206] whereas crack propagation is continuous in bicrystals[208].

Dynamic intergranular fracture, (or "dynamic embrittlement") has been documented for both oxygen and sulphur migrating to copper grain boundaries under applied tensile stress[207, 321]. This has important consequences, since copper alloys are, therefore, potentially susceptible to subcritical cracking phenomena, particularly when heated in air.

It is interesting to note that both fracture by dynamic embrittlement, and the ductility trough phenomenon in general, disappear at high strain-rates. In the former mechanism this is simply because the segregant needs time to diffuse to sites of stress concentration[206], while in the latter this occurs for reasons exposed above. The observation that embrittlement of copper or one of its alloys disappears at high strain rates is therefore not to be taken as a signature of dynamic embrittlement, even if an embrittling segregant is present: such behaviour is also a feature of the conventional grain boundary embrittlement of copper and its alloys.

Liquid Metal Embrittlement

Suppose now that the crack faces are in contact with a liquid: this introduces two fundamental changes. The first is that the local work of cohesion is changed, since this now becomes:

$$\gamma_{int} = 2\,\gamma_{SL} - \gamma_{GB} \qquad \text{Eq. 3}$$

where γ_{SL} is the solid/liquid interfacial energy and γ_{GB} the grain boundary energy (for intergranular fracture; $\gamma_{int} = 2\,\gamma_{SL}$ for transgranular fracture).

The second is that the presence of the liquid shifts the kinetics of dynamic embrittlement phenomena to far more rapid regimes, because diffusion through liquids is comparatively rapid and also because a wetting liquid metal can infiltrate cracks rapidly (with liquid metals, surface forces are high and viscosities are low compared with other infiltrants[322]). As a result, contact of many metals - and copper is no exception - with another metal in the molten state can lead to fracture under stresses well below those observed in the absence of the molten metal; hence, the great engineering importance of LME.

Liquid metal embrittlement can be revealed and studied using both tensile and fracture toughness testing. Many of the tests performed in order to determine LME susceptibility of copper and its alloys are made by placing the solid metal in contact with the liquid metal, either in a bath, or held as a pendular drop contacting a groove. Such tests are delicate and often lead to erratic, or falsely negative, results because they require perfect contact between the two metals, which is not always easy to bring about. Good wetting of the solid by the liquid requires a low contact angle, and oxides covering the metal often interfere with the wetting process[300, 306, 308, 323-326]. For example, in Ref.[327], the liquid metal embrittlement susceptibility of a martensitic steel by Pb-Bi is shown to depend strongly on the intimate contact requirement: there is an apparent

change in the fracture mode from ductile to brittle only when the natural oxide barrier protection is carefully suppressed.

In tensile testing, liquid metal embrittlement leads to the appearance of a marked ductility trough[298, 301, 302] for which T_E is generally situated at the melting point of the embrittling metal; however, exceptions exist to this rule. These exceptions occur either because of embrittler undercooling[1] (when it takes the form of submicrometric inclusions within the solid metal) or because solid metal induced embrittlement is also active below the embrittler melting temperature. It has been stated that, for LME to appear, the applied stress must generate at least localised plastic deformation in the solid metal[298, 301, 302, 306]. Crack initiation is furthermore driven by the presence of stress-concentrating obstacles to slip[298]. There are also data to show that in metals embrittled by LME, eased plastic deformation is observed[302].

Liquid metal embrittlement bears strong similarities with other environmental embrittlement phenomena, including stress-corrosion cracking or hydrogen-assisted cracking[298, 304]. In particular, the relation between crack velocity and the crack stress intensity factor is similar between LME and these other environmental embrittlement phenomena: there is a threshold stress intensity, $K_{1\,LME}$, below which cracks do not grow and slightly above which the rate of crack growth increases steeply with increasing K until a plateau is reached, the plateau extending until K reaches the critical stress intensity factor for rapid fracture of the material. In LME, however, there is the significant difference with other environmental cracking phenomena that the plateau cracking velocity is very high[301, 306, 328]. This is because the supply of liquid metal to a moving crack tip is rapid, being limited, all the way up to the crack tip, only by viscous flow. Liquid metals have comparatively low viscosities[322]; hence, this limit is not very stringent: it can be estimated to be on the order of a centimetre per second to even several meters per second[329] (depending on the estimation and the system). Additionally, all these environmental embrittlement phenomena have common fractographic signatures[304].

By and large, the response to metallurgical and test variables of systems subject to liquid metal embrittlement parallels that which is observed in low-temperature plasticity and fracture of brittle metallic materials[299, 302]. Liquid metal embrittlement is, in other words, promoted by all factors that tend to increase the intensity of local stress concentration caused by slip, particularly - but not only - at grain boundaries[302]. Trends are thus that the severity of embrittlement, meaning in LME both the trough depth and the brittle-to-ductile transition temperature T_R (since the ductile-to-brittle transition T_E is generally fixed at the embrittler melting point) increase as the solid (embrittled) metal hardness is increased and as the propensity for local stress concentration

created by slip is increased. Precipitation hardening, a decrease in stacking fault energy, and cold work in the embrittled metal thus all tend to increase the level of embrittlement[299, 302].

The role of grain size is, once again, less clear: although a larger grain size reduces the material flow stress, it also can increase the level of local stress concentration within the material (as dislocation pile-ups become longer). It has thus been found that the metal fracture stress can follow the Hall-Petch behaviour in the presence of MIE[302], but contradictory data have been recorded regarding the influence of grain size and cold work[301, 302].

Following these general trends, the severity of embrittlement also increases as the strain rate increases[298, 301, 302, 330]. In this regard, LME therefore differs radically from grain boundary embrittlement induced ductility trough behaviour, in particular as observed for copper and its alloys (see above). Examples of such behaviour in leaded brasses can be found in Refs.[331, 332].

For LME, the upper, brittle to ductile, transition at T_R is therefore interpreted as being mostly a simple result of the general increase in metal ductility that accompanies an increase in temperature. In general, thus, T_R tends to increase with increasing strain rate, with decreasing grain size[298], and with the onset of grain boundary mobility[330] when the trough is governed by liquid metal embrittlement.

Copper and its alloys are embrittled by liquid Sn, Pb, Bi, Pb-Bi, Sn-Pb, Pb-Ag, Hg, Ga, Ga-In, Ga-Hg, In, In-Hg, Zn, Li, Na, Sb, Th [260, 298, 301, 309, 328, 331, 333-343]. Low melting point embrittler metals typically have little or no mutual solubility with copper and form no intermetallics (as is typical of embrittled/embrittling MIE metal pairs; see above); however, exceptions exist to this rule[302]. Although embrittlement of one metal by another is an atom-to-atom phenomenon that is hard to suppress, some strategies have been proposed to reduce its severity. One example is given by phosphorus additions to Monel against embrittlement by mercury[298, 344].

Since it generally is insoluble and forms no intermetallic, the embrittling liquid metal can also come in contact with copper or its alloys from within, as an inclusion situated inside the metal. This situation, often encountered in practice, is also convenient from a testing standpoint because it alleviates difficulties associated with causing the liquid embrittler to wet the metal along its outer surface (see above). The principal practical example of this in copper is with lead; Fig. 16 gives an example of a leaded copper alloy, showing typical intergranular lead inclusions. Copper alloys containing a few percent lead have microstructures in which the lead takes the form of small inclusions, many of which are situated along grain boundaries. Figure 17 gives an illustration of the fracture surface along a quench-crack formed during the excessively rapid quenching of a high-strength Cu-Ni-Sn alloy containing liquid lead inclusions (which have,

therefore, moved away from their original location along the fracture surface). The sharpness of this fracture surface betrays the elevated brittleness of the material at the time of cracking.

In practice, lead is added to copper alloys because it increases significantly their ease of machining[1, 345]. Leaded brasses are a typical example of free-machining copper alloys, Alloy C36000 (CuZn36Pb3) being the reference free-machining brass; however, many other leaded copper alloys exist. Their number and production volume is declining because of the health hazards posed by lead, which in turn has motivated legislation to gradually ban their production and usage (*e.g.*, European Union directives on electronic equipment[346, 347] and the automotive industry[348], as well as legislation limiting the quantity of lead leached into drinking water and therefore affecting plumbing system component requirements[349, 350]).

One of the most active areas of current R&D in copper alloys is, as a consequence, the search for alternatives to lead in free-machining alloys. The most obvious substitute is another well-known low-melting point embrittler, namely bismuth, which is presently used as a replacement for lead in water-plumbing brasses[351]. Bismuth, however, has the disadvantage that it is a very strong embrittler of grain boundaries also in the solid state; as a consequence it weakens copper alloys quite considerably in practice[352]. Bismuth of course also poses serious problems as a tramp element in recycling.

An important parameter in liquid metal embrittlement is the dihedral angle, ϕ, defined in Fig. 18. Once it is substituted in Eq. 3, the local work of fracture becomes:

$$\gamma_{int} = 2\ \gamma_{SL}\ [1 - \cos(\phi/2)]\ . \qquad \text{Eq. 4}$$

Hence, the lower the dihedral angle is, the lower the work of fracture becomes in the presence of the liquid at given liquid/solid interfacial energy.

Measurements of dihedral angles are conducted using one of three methods: (i) two-dimensional metallography coupled with statistical and stereological analysis (*e.g.*, Ref.[353]), (ii) two or three-dimensional analysis of the shape of grooves created where the liquid metal wets a surface that is intersected by a grain boundary, interpreted using Mullins's analysis of this situation (*e.g.*, Ref.[354]) (iii) transmission electron microscopy of submicronic inclusions (*e.g.*, Ref.[355]) and (iv) a recent three-dimensional image analysis method developed for lead inclusions in copper (Refs.[129, 356]). The last three methods differ from the first in that they yield individual, rather than average, dihedral angle values. Measurement of individual values shows that the dihedral angle in fact varies greatly with the grain boundary character. A corollary is that, also for resistance to embrittlement by LME, grain boundary engineering holds great promise.

It is known that under tensile stress liquid inclusions, including liquid lead in copper alloys, may change their shape: this occurs because under stress, the equilibrium shape of the inclusion

is that which minimises, not just the total capillary energy, but the sum of capillary and stored elastic energy within the solid/liquid material. Under tensile stress, inclusions therefore redistribute matter so as to become aligned perpendicularly to the stress direction, while inclusions already perpendicular to the stress direction tend to flatten[129, 260, 357-360]. Liquid inclusions also tend, in the presence of applied stress, to increase the amount of damage caused by grain boundary sliding[361, 362].

At sufficiently high levels of stress, the inclusions may become unstable, particularly if under tensile stress pore nucleation occurs within the inclusion. For the simple case of a circular isolated grain boundary inclusion in a linear elastic solid of Young's modulus E, expressions have been proposed to predict the stress σ above which such unstable inclusion spreading occurs[357, 363]. These predict fracture when a dimensionless parameter Λ (*), defined as:

, Eq. 5

exceeds a ϕ-dependent critical value that decreases as ϕ decreases. V is the inclusion volume: larger inclusions, lower liquid/solid interfacial energies (and hence segregants within the liquid) and lower dihedral angles thus lead to greater brittleness above the embrittler melting point. This result is, in essence, a Griffith-type criterion grounded in the basic, Rehbinder (surface energy reduction) interpretation of liquid metal embrittlement[364-366].

Note: (*: please note that there is a typo, namely the exponent two missing on the applied stress, in the corresponding equation as well as in the equation defining the elastic energy $U_{elastic}$ on page 611 of Ref. [363])

Competition between mechanisms: the case of leaded copper

It is interesting to note that liquid metal embrittlement displays parametric dependencies that differ notably from those of trough behaviour dictated by solid-state creep-cavitation. It may, therefore, be possible to discriminate between mechanisms by close examination of how a parameter, notably the strain rate, affects the ductility trough. Leaded copper alloys represent an interesting example of this: data suggest that both mechanisms, grain boundary embrittlement and liquid metal embrittlement, are operative, that which dominates being a function of circumstances.

It has been argued on the basis of thermodynamic analysis of dihedral angle data that there is no lead segregation to Cu grain boundaries[11, 259]. Still, lead is clearly a grain boundary embrittler, see Fig. 19. At average lead contents as low as 18 ppm [10, 367], significant embrittlement of Cu-Ni alloys is indeed observed (the room temperature solubility of Pb in Cu is estimated at below 100 ppm [367]). Significant (grain boundary) embrittlement also results after solid state penetration of the alloy by lead gas from its outer surface at 800°C [368]. All these data show that lead causes solid-state grain boundary embrittlement in copper. This is also suggested by the strain-rate dependence of the ductility trough that is reported for strain rates below impact testing in Ref.[150] for α-brasses containing 50 and 900 ppm lead: the trough widens as the strain rate decreases.

On the other hand, it is also clear from the literature that lead causes liquid and solid metal embrittlement of copper and its alloys[31-33, 260, 298]. This is suggested by the influence of strain rate on ductility in other data sets[330]. Figures 20 and 21 illustrate this for Cu-1wt.%Pb [129]. The ductility trough of OFHC copper, which is clearly visible at low strain rates and disappears when the metal is tested at 10 s^{-1}, Fig. 20 (see also Fig. 6, bottom graph), is also observed for the leaded alloy at the higher strain rate of 10 s^{-1}. There is no extensive damage accumulation along the fracture surface of rapidly strained leaded copper, Fig. 21, while at low strain rates, there is significant intergranular voiding and decohesion. The material fails by propagation of a single crack along grain boundaries, with occasional branching, also along grain boundaries. The tensile curve is also characteristic of liquid metal embrittlement: the curve follows quite precisely that of the non-leaded metal and then stops abruptly well before the maximum stress observed in the absence of lead[129].

In leaded copper, depending on testing conditions, there are thus two causes for ductility trough behaviour: (i) intergranular voiding, exacerbated by the presence of lead as a grain boundary segregant, and (ii) liquid metal embrittlement, also caused by lead but in the form of liquid intergranular inclusions (or in some instances as a medium that the alloy contacts along its outer surface). This complexity of the ductility trough behaviour of leaded copper has, in fact, been at the origin of some controversy, in which both one[1, 260], and the other[11, 259], view of the phenomenon was apparently justified.

Conclusion

Intermediate temperature embrittlement, also named ductility trough behaviour, is a phenomenon that has major importance in the processing and elevated temperature behaviour of copper and its alloys. It has two possible causes and mechanisms.

The first is intergranular creep cavitation; this mechanism is dominant at low strain rates. Being a basic embrittlement mechanism, present even in high-purity copper, it is difficult to avoid; however, it is strongly influenced by several factors and can thus be reduced. Prime among these are (i) avoiding the presence of grain boundary segregants that weaken grain boundaries, (ii) favouring rapid deformation, (iii) using alloying additions that scavenge unfavourable impurities and/or strengthen grain boundaries, and (iv) adding second phases that strengthen the material against cavitation along grain boundaries.

Metal-induced embrittlement, and particularly liquid metal embrittlement, is a potential second cause for intermediate temperature embrittlement in some copper alloys, particularly those containing lead or bismuth above the melting point of these two metals. Here, the phenomenon has different causes, and responds when liquid metal is present to deformation parameters in a manner that parallels low-temperature, instead of high-temperature, ductile fracture. Strategies for the minimisation of embrittlement will then depend on whether the embrittler is liquid or solid.

In all cases, embrittlement is linked with the presence of grain boundary weakness and cracking: it is the localisation of damage and crack propagation at the grain boundaries that causes the material to fail at low strain. More radical strategies towards avoiding, or minimising, the phenomenon must therefore be ones that alter dramatically the nature and distribution of grain boundaries while, at the same time, preserving the metal or alloy performance in terms of strength or toughness. One method may be to introduce a significant fraction of second phase that replaces a large fraction of grain boundaries with interphase boundaries that are more resistant to cavitation and fracture than copper grain boundaries. This "composite" strategy poses however the challenge that only few realistic second phases will preserve the room-temperature ductility of copper or α-copper alloys. An alternative strategy is to alter radically the nature of the grain boundaries in a monophase copper alloy. This approach, currently called "grain boundary engineering" [281], holds significant promise for progress because it tackles the issue at its root, in a manner that is radical yet remains compatible with current approaches to copper alloy design and processing.

Acknowledgements

This article is an outgrowth of a research collaboration between the authors' laboratory and the Swiss company Swissmetal (Dornach, Switzerland), co-sponsored by Swissmetal and the Swiss Commission for Technology and Innovation (CTI), Project Number 6668.2 IWS-IW. Our many enlightening discussions with colleagues at Swissmetal in both Dornach and Reconvilier,

particularly Dr. Claudio Penna, Dr. Emmanuel Vincent, Dr. Natanael Dewobroto, Dr. Christian Charbon, Dr. Peter Isler and Dr. Bernard de Mestral, are gratefully acknowledged, as are discussions with Dr. Massoud Dadras of the University of Neuchatel during this collaboration. We thank Dr. Ozgowicz for permission to reproduce Fig. 11 from his work, and Dr. Eustathopoulos both for permission to reproduce Fig. 19(a) from his work, and for his encouragement to publish this review as well as for interesting discussions on this topic. Several of the figures presented here are from the doctoral thesis of Dr. Laurent Felberbaum (formerly of our laboratory and now with Sécheron S.A. in Geneva, Switzerland) whom we thank warmly for granting us permission to reproduce these in this review and also for many years' fruitful collaboration and numerous stimulating discussions on the general subject of this review.

List of figures captions:

Figure 1 - Reduction in area versus deformation temperature in tensile testing of OFHC copper: empty circles from data gathered under vacuum at $4.6x10^{-4}$ s^{-1} on OFHC copper of average grain size 300-400 μm by Suzuki and Itoh[186]; full circles from data gathered under argon at $1x10^{-3}$ s^{-1} on OFHC copper of average grain size 150 μm by Ozgowicz and Biscondi[174]; empty squares from data gathered under argon at 10^{-3} s^{-1} on OFHC copper of average grain size 150 μm by Sanchez-Medina et al.[259] and full triangles from data gathered under vacuum at roughly 10^{-3} s^{-1} on OFHC copper of average grain size 100 μm by Davies and al.[6].

Figure 2a – General shape and features of the ductility trough (after Refs.[6, 11]);

Figure 2b – Sketch of the shape of tensile curves in relation to Fig. 3a (after Refs.[6, 11]);

Figure 2c – Fractured surface of tensile specimens of OFHC copper tested at 20°C at a strain rate of 10^{-4} s^{-1};

Figure 2d – Fractured surface of tensile specimens of OFHC copper tested at 450°C at a strain rate of 10^{-4} s^{-1};

Figure 2e – Fractured tensile specimens of OFHC copper tested at a strain rate of 10^{-4} s^{-1} (round bars with a Ø4 mm initial diameter) .

Figure 3 – Two different examples of cracks formed as a result of embrittlement of copper-nickel based alloys ; top: longitudinal cracks caused by residual stresses; bottom: spiral-shaped crack formed during extrusion (courtesy of Swissmetal®, Dornach, Switzerland).

Figure 4a - The fracture mechanism map for OFHC copper (redrawn from Ref.[14]);

Figure 4b - The deformation mechanism map for OFHC copper (redrawn from Ref.[120]): strain rates refer to constant secondary creep rates;

Figure 4c - Constant secondary creep rate curves (redrawn from Ref.[120]) superimposed on the fracture mechanism map (redrawn from Ref.[14]) together with experimental data points: full

symbol denotes brittle intergranular fracture, empty symbols denote ductile rupture, squares from data gathered at 10^{-4} s^{-1} by Felberbaum[129] on OFHC copper of average grain size 25 μm, circles from data gathered at 10 s^{-1} by Felberbaum[129] on OFHC copper of average grain size 25 μm, diamonds from data gathered at 4.4×10^{-3} s^{-1} by Igata et al.[128] on OFHC copper of average grain size 50 μm, showing the ductility trough (with DF: Ductile Fracture, TCF: Transgranular Creep Fracture and DRX: Dynamic Recrystallisation);

Figure 4d - The influence of grain size d on the transition in dominance of diffusive creep (below black lines indexed with discrete values for d) versus power-law creep (above previously mentioned black lines) after Ref.[120] (with ICF: Intergranular Creep Fracture). The quasi-horizontal dotted line is the low limit for Power-Law Breakdown while the other (curved) dotted line separates High and Low Temperature Power-Law creep (see Fig. 4b, which is plotted for d=100μm).

Figure 5 - Sketched flow curves in the presence of dynamic recrystallisation with an indication of the influence of the initial grain size, plus that of temperature T and strain rate combined into the Zener-Hollomon parameter , with Q, the activation energy and k, Boltzman's constant (after Sakai and Jonas[70]).

Figure 6 - Ductility trough variation as a function of strain rate. Top: after Ref.[6]; squares from data gathered at roughly 10^{-1} s^{-1}, diamonds for data gathered at roughly 10^{-2} s^{-1}, triangles for data gathered at roughly 10^{-3} s^{-1} and circles for data gathered at roughly 10^{-4} s^{-1} on OFHC copper of average grain size 100 μm). Middle graph after Ref.[127]; squares for data gathered at 120 s^{-1}, diamonds for data gathered at 2.8×10^{-1} s^{-1}, triangles for data gathered at 2.3×10^{-2} s^{-1} and circles for data gathered at 2.3×10^{-3} s^{-1} on OFHC copper of average grain size 80 μm. Bottom: after Ref.[129]; full symbols denote 4N Copper; empty symbols denote OFHC Copper, circles for data gathered at 10^{-4} s^{-1}, squares for data gathered at 10 s^{-1} on copper of average grain size 25 μm.

Figure 7 - Longitudinal cuts across the tensile fracture surface of round bars of OFHC copper, tested at (a) 10 s^{-1} and (b) 10^{-4} s^{-1} (RA = Reduction in Area); as seen, fracture at the lower strain rate is accompanied by extensive internal damage development (from Felberbaum[129]).

Figure 8 - Redrawn from Mohamed and Langdon[142] where the normalised creep rate is defined as

(: steady state creep rate, *k*: Boltzman's constant, *T*: temperature, *D*: Herring-Weertman weighted diffusion coefficient, *G*: shear modulus and *b*: Burgers' vector length) and the stacking fault energy γ is normalised by *Gb*; data were obtained for an applied stress of 2.10^{-4} *G*.

Figure 9 - Influence of zinc content on the ITE of α-brass at 400 and 500°C (after Ohmori[126, 143] and Shibayanagi[126, 143]).

Figure 10 – Ductility trough in pure (full symbols) and internally oxidised (hollow symbols) polycrystalline copper with two different strain rate: circles are from data gathered at roughly 10^{-1} s^{-1} and triangles from data gathered at roughly 10^{-3} s^{-1}; grain size is around 100 μm (after Davies et al.[6]).

Figure 11 - Reduction in area versus deformation temperature and grain size of industrial bronze CuSn6 stretched at a strain rate of 1.19×10^{-3} s^{-1}. Figure reproduced from Ozgowicz[3], with permission from Elsevier Ltd.

Figure 12 - Ductility troughs in OFHC (Oxygen Free High Conductivity, i.e. 3N5) Copper (containing 6ppm of sulphur) and OSFC (Oxygen and Sulphur Free: sulphur concentration less than 1ppm) Copper after Suzuki[186] (tests conducted in vacuum at 4.6×10^{-4} s^{-1}), and in copper of varying purity after Fujiwara[185] (tests conducted in vacuum at 4.2×10^{-5} s^{-1}).

Figure 13 - Sublimation enthalpy of 33 elements redrawn from Seah[196]; full symbols are known embrittlers of copper.

Figure 14 - Periodic table of the elements indicating in black known embrittlers of copper, and in bold-italics known "de-embrittlers" of copper.

Figure 15 - (a) segregated grain boundary submitted to a tensile stress with a constant grain boundary segregant concentration Γ_0^{gb}; (b) rapid fracture of the grain boundary: the impurity global segregation level is unchanged and the segregant chemical potential μ is therefore not

uniform; (c) quasistatic fracture of the grain boundary; here the free surface concentration Γ_0^s is dictated by equalisation of the segregant chemical activity μ across the sample; (d) dynamic embrittlement comprising diffusion-controlled stress-induced segregant concentration changes at the crack tip.

Figure 16 – Polished section of a Cu-1Pb sample heat treated at 900 °C 1 h and 400 °C 24 h; selected lead inclusions are indicated by arrows (from Felberbaum[129]).

Figure 17 - Sharp intergranular fracture surface along a quench crack in an experimental high-strength Cu-Ni-Sn-Pb alloy (from Felberbaum[129]).

Figure 18 - Schematic view of an equilibrated lenticular inclusion situated along a planar grain boundary: (a) 3D view, and (b) detail: the cut is perpendicular to both the grain boundary plane and the triple line (from Felberbaum[129]).

Figure 19 - Effect of lead additions on ductility-temperature behaviour of OFHC copper (a) and high-purity Cu-10Ni alloy (b). Figure 19(a) reprinted from Sanchez Medina, Sangiorgi and Eustathopoulos [259] with permission from Elsevier Ltd. Figure 19(b) reprinted from Gavin, Billingham, Chubb and Hancock[10] with permission from Maney Publishers/the Institute of Materials.

Figure 20 - Reduction in area of leaded and unleaded pure OFHC copper after elevated temperature tensile testing at two different strain rates; from Felberbaum[129]. Square symbols denote tests conducted at a strain rate of 10^{-4} s^{-1}, while round symbols are for tests conducted at 10 s^{-1}. Filled symbols are for Cu-1wt.%Pb. Arrows are added in order to help direct comparison between unleaded and leaded material under the same test conditions.

Figure 21 - Longitudinal cuts across the tensile fracture surface of round bars of Cu-1wt.%Pb, tested at (a) 10 and (b) 10^{-4} s^{-1} (RA = Reduction in Area), denoting the presence of extensive damage at the lower strain rate, and of sharp intergranular fracture at the higher strain rate (from Felberbaum[129]; this figure is to be compared with Fig. 7).

References

1. M. C. Roth, G. C. Weatherly, and W. A. Miller: Can. Metall. Q., 1979, 18, 341-348.
2. D. J. Wolley and A. G. Fox: J. Mater. Sci. Lett., 1988, 7, 763-765.
3. W. Ozgowicz: J. Mater. Process. Technol., 2005, 162-163, 392-401.
4. J. N. Greenwood, D. R. Miller, and J. W. Suiter: Acta Metall., 1954, 2, 250-258.
5. M. Ohmori and K. Wakasa: J. Jpn. Inst. Met., 1973, 37, 1195-1199.
6. P. W. Davies, G. R. Dunstan, R. W. Evans, and B. Wilshire: J. Inst. Met., 1971, 99, 195-197.
7. H. Yamagata and O. Izumi: J. Jpn. Inst. Met., 1978, 42, 1012-1019.
8. S. Sato, T. Otsu, and E. Hata: J. Inst. Met., 1970, 98, 135-141.
9. B. J. Reid and J. N. Greenwood: Trans. Metall. Soc. AIME, 1958, 212, 503-507.
10. S. A. Gavin, J. Billingham, J. P. Chubb, and P. Hancock: Met. Technol., 1978397-401.
11. M. Sanchez Medina, R. Sangiorgi, L. Coudurier, and N. Eustathopoulos: Mem. Et. Sci. Rev. Metall., 1981, 78, 101-109.
12. M. Kanno: Z. Metall., 1988, 79, 684-688.
13. H. J. McQueen: 'Hot workability and thermo-mechanical processing of copper alloys', Copper'91, Ottawa (Canada), 1991, Pergamon Press, 281-295.
14. M. F. Ashby, C. Gandhi, and D. M. R. Taplin: Acta Mater., 1979, 27, 699-729.
15. H. J. McQueen: 'Dynamic Recovery and Recrystallization', in 'Encyclopedia of Materials: Science and Technology', (ed. K. H. J. Buschow, R. W. Cahn, M. C. Flemings, B. Ilschner, E. J. Kramer, and S. Mahajan), 2375-2381; 2001, Oxford, Elsevier Science Ltd.
16. B. Mintz, S. Yue, and J. J. Jonas: Int. Mater. Rev., 1991, 36, 187-217.
17. R. F. Higgins: 'Engineering Metallurgy - Applied Physical Metallurgy 6th edition'; 1993, London (UK), Edward Arnold.
18. D. Arnaud, J. Barbery, R. Biais, B. Fargette, and P. Naudot: Tech. Ing. Mater. Met., 1985, M 430, 1-45.
19. R. Carlsson: Scand. J. Metall., 1980, 9, 25-29.
20. K. I. Hanser: Z. Metall., 1926, 18, 247-255.
21. R. V. Foulger and E. Nicholls: Met. Technol., 1976, 3, 366-369.
22. R. Hannesen, U. Heubner, and V. Schumacher: Z. Metall., 1967, 58, 423-433.
23. Anon.: Metallurgia, 1995, 62.
24. M. Cook and E. Davis: J. Inst. Met., 1950, 76, 501-526.
25. J. J. Cronin: 'Selecting High Conductivity Copper-Alloys for Elevated-Temperature Use', in 'Source Book on Materials Selection', 222-230, 1977, Metals Park (OH), American Society for Metals.
26. C. S. Smith: Trans. Am. Inst. Min. Metall. Eng., 1948, 175, 15-51.
27. K. Dies: 'Kupfer und Kupferlegierungen in der Technik'; 1967, Springer-Verlag.
28. A. Couture: Trans. Am. Found. Soc., 1966, 74, 709-721.
29. G. Pantazopoulos and A. Vazdirvanidis: J. Fail. Anal. Prev., 2008, 8, 218-222.
30. M. Yamamoto and T. Mizuguchi: Can. Metall. Q., 1999, 38, 387-396.
31. P. Isler and W. Form: J. Inst. Met., 1972, 100, 107-113.
32. H. W. Schläpfer and W. Form: Met. Sci., 1979, 13, 13-19.
33. W. Form, N. Peguiron, and B. Furrer: Mem. Et. Sci. Rev. Metall., 1982, 79, 143-148.
34. D. F. Lupton and J. R. Thompson: J. Inst. Met., 1972, 100, 352-356.
35. M. V. Zakharov: Weld. Prod., 1985, 5, 43-45.
36. G. Pantazopoulos: J. Fail. Anal. Prev., 2003, 3, 14-22.
37. D. Padmavardhani and Y. V. R. K. Prasad: Mater. Sci. Eng., A, 1992, 157, 43-51.
38. N. Ravichandran and Y. V. R. K. Prasad: Mater. Sci. Eng., A, 1992, 156, 195-204.
39. N. Ravichandran and Y. V. R. K. Prasad: Z. Metall., 1993, 84, 132-139.

40. D. Padmavardhani and Y. V. R. K. Prasad: J. Mater. Sci., 1993, 28, 5269-5274.
41. D. Padmavardhani and Y. V. R. K. Prasad: J. Mater. Sci., 1993, 28, 5275-5279.
42. Z. Gronostajski: Arch. Metall., 2001, 46, 351-360.
43. Z. Gronostajski: J. Mater. Process. Technol., 2002, 125, 119-124.
44. Z. Gronostajski: J. Mater. Process. Technol., 2005, 159, 377-382.
45. Y. V. R. K. Prasad and K. P. Rao: Mater. Sci. Eng., A, 2005, 391, 141-150.
46. Y. V. R. K. Prasad and K. P. Rao: Mater. Sci. Eng., A, 2005, 391, 141-150.
47. Y. V. R. K. Prasad and K. P. Rao: Mater. Lett., 2006, 60, 2786-2790.
48. Y. V. R. K. Prasad and K. P. Rao: J. Eng. Mater. Technol., 2006, 128, 158-162.
49. D. J. Edwards, B. N. Singh, Q. Xu, and P. Toft: J. Nucl. Mater., 2002, 307, 439-443.
50. S. A. Fabritsiev and A. S. Pokrovsky: J. Nucl. Mater., 2007, 367, 977-983.
51. S. A. Fabritsiev and A. S. Pokrovsky: Plasma Devices and Operations, 2008, 16, 67-73.
52. B. N. Singh, D. J. Edwards, M. Eldrup, and P. Toft: J. Nucl. Mater., 1997, 249, 1-16.
53. M. F. Ashby: Adv. Appl. Mech., 1983, 23, 117-177.
54. D. M. R. Taplin, G. Chimata, and M. F. Ashby: Eng. Fract. Mech., 1979, 11, 458-458.
55. D. Teirlinck, F. Zok, J. D. Embury, and M. F. Ashby: Acta Metall., 1988, 36, 1213-1228.
56. M. E. Kassner and T. A. Hayes: Int. J. Plast, 2003, 19, 1715-1748.
57. A. C. F. Cocks and M. F. Ashby: Prog. Mater Sci., 1982, 27, 189-244.
58. M. F. Ashby and B. F. Dyson: 'Creep damage mechanisms and micromechanisms in "Advances in Fracture Research"', Fracture (6th International Conference), New Delhi (IN), 1984, Pergamon Press, 3-30.
59. M. E. Kassner and M. T. Perez-Prado: 'Chapter 10 - Creep fracture', in 'Fundamentals of creep in metals and alloys', 215-241, 2004, Amsterdam (NL), Elsevier.
60. T. Watanabe and P. W. Davies: Philos. Mag. A, 1978, 37, 649-681.
61. T. Watanabe: Metall. Trans. A, 1983, 14A, 531-545.
62. S. Afshar and M. Biscondi: Scr. Metall., 1986, 20, 707-711.
63. S. V. Raj: J. Mater. Sci., 1991, 26, 1000-1008.
64. H. D. Chandler: Mater. Sci. Eng., A, 1993, 169, 27-32.
65. A. Ayensu and T. G. Langdon: Metall. Trans. A, 1996, 27, 901-907.
66. H. Yamagata and O. Izumi: J. Jpn. Inst. Met., 1978, 42, 1096-1103.
67. L. C. Lim: Acta Metall., 1987, 35, 1663-1673.
68. T. Shibayanagi, A. Yoshimoto, and S. Hori: Mater. Trans., JIM, 1990, 31, 1057-1064.
69. R. Raj and M. F. Ashby: Acta Metall., 1975, 23, 653-666.
70. T. Sakai and J. J. Jonas: Acta Metall., 1984, 32, 189-209.
71. G. Gottstein and U. F. Kocks: Acta Metall., 1983, 31, 175-188.
72. P. Karduck, G. Gottstein, and H. Mecking: Acta Metall., 1983, 31, 1525-1536.
73. V. M. Sample, G. L. Fitzsimons, and A. J. Deardo: Acta Metall., 1987, 35, 367-379.
74. W. Bochniak and M. Niewczas: Z. Metall., 1993, 84, 211-215.
75. W. Bochniak and M. Niewczas: Z. Metall., 1994, 85, 733-737.
76. J. Takada, N. Nishino, and S. Kikuchi: J. Mater. Sci., 1986, 21, 3420-3424.
77. H. Miura, M. Ozama, R. Mogawa, and T. Sakai: Scr. Mater., 2003, 48, 1501-1505.
78. H. Miura, T. Sakai, R. Mogawa, and G. Gottstein: Scr. Mater., 2004, 51, 671-675.
79. H. Miura, T. Sakai, H. Hamaji, and J. J. Jonas: Scr. Mater., 2004, 50, 65-69.
80. H. Miura, T. Sakai, S. Andiarwanto, and J. J. Jonas: Philos. Mag., 2005, 85, 2653-2669.
81. H. Miura, T. Sakai, and J. J. Jonas: Scr. Mater., 2006, 55, 167-170.
82. H. J. McQueen and S. Bergerson: Met. Sci. J., 1972, 6, 25-29.
83. M. Ueki and T. Nakamura: J. Jpn. Inst. Met., 1977, 41, 50-54.
84. R. A. Petkovic, M. J. Luton, and J. J. Jonas: Acta Metall., 1979, 27, 1633-1648.
85. M. J. Luton, R. A. Petkovic, and J. J. Jonas: Acta Metall., 1980, 28, 729-743.
86. J. Hennaut, J. Othmezouri, and J. Charlier: Z. Metall., 1982, 73, 744-753.
87. L. Blaz, T. Sakai, and J. J. Jonas: Met. Sci., 1983, 17, 609-616.

88. L. Blaz and A. Korbel: Mater. Sci. Technol., 1989, 5, 1186-1190.
89. S. R. Chen and U. F. Kocks: Scr. Metall. Mater., 1992, 27, 1587-1592.
90. L. C. Lim and H. H. Lu: Mater. Sci. Eng., A, 1994, 176, 439-446.
91. A. Belyakov, W. Gao, H. Miura, and T. Sakai: Metall. Mater. Trans. A, 1998, 29, 2957-2965.
92. W. Gao, A. Belyakov, H. Miura, and T. Sakai: Mater. Sci. Eng., A, 1999, 265, 233-239.
93. A. Manonukul and F. P. E. Dunne: Acta Mater., 1999, 47, 4339-4354.
94. A. Rohatgi, K. S. Vecchio, and G. T. Gray: Metall. Mater. Trans. A, 2001, 32, 135-145.
95. A. M. Wusatowska-Sarnek, H. Miura, and T. Sakai: Mater. Sci. Eng., A, 2002, 323, 177-186.
96. Y. V. R. K. Prasad and K. P. Rao: Mater. Sci. Eng., A, 2004, 374, 335-341.
97. V. G. Garcia, J. M. Cabrera, and J. M. Prado: Recrystallization and Grain Growth, Pts 1 and 2, 2004, 467-470, 1181-1186.
98. A. M. Wusatowska-Sarnek: J. Eng. Mater. Technol., 2005, 127, 295-300.
99. M. Dollar, S. Dymek, S. J. Hwang, and P. Nash: Metall. Trans. A, 1993, 24, 1993-2000.
100. H. J. Mcqueen and C. A. C. Imbert: J. Alloys Compd., 2004, 378, 35-43.
101. N. Srinivasan and Y. V. R. K. Prasad: Mater. Sci. Technol., 1992, 8, 206-212.
102. L. Benmostefa, G. Saindrenan, M. P. Solignac, and J. P. Colin: Acta Metall. Mater., 1991, 39, 3111-3118.
103. S. V. Raj and T. G. Langdon: Acta Metall., 1989, 37, 843-852.
104. S. V. Raj and T. G. Langdon: Acta Metall. Mater., 1991, 39, 1817-1822.
105. S. V. Raj and T. G. Langdon: Acta Metall. Mater., 1991, 39, 1823-1832.
106. P. J. Henderson and R. Sandstrom: Mater. Sci. Eng., A, 1998, 246, 143-150.
107. R. G. Fleck, G. J. Cocks, and D. M. R. Taplin: Metall. Trans., 1970, 1, 3415-3420.
108. H. H. Bleakney: Can. Metall. Q., 1965, 4, 13-29.
109. J. E. Benci, D. P. Pope, and J. L. Bassani: Acta Metall. Mater., 1994, 42, 225-238.
110. G. J. Cocks and D. M. R. Taplin: Scr. Metall., 1969, 3, 623-626.
111. B. Wilshire and C. J. Palmer: Scr. Mater., 2002, 46, 483-488.
112. S. V. Raj and T. G. Langdon: J. Met., 1983, 35, 99-99.
113. B. Wilshire, H. Burt, and A. J. Battenbough: Mater. Sci. Eng., A, 2005, 410, 16-19.
114. B. Wilshire and C. J. Palmer: Mater. Sci. Eng., A, 2004, 387-89, 716-718.
115. S. G. R. Brown, R. W. Evans, and B. Wilshire: Mater. Sci. Technol., 1987, 3, 23-27.
116. J. D. Parker and B. Wilshire: Mater. Sci. Eng., 1980, 43, 271-280.
117. A. Ayensu, G. K. Quainoo, and S. K. Adjepong: J. Mater. Sci. Lett., 1993, 12, 1008-1010.
118. B. Wilshire and A. J. Battenbough: Mater. Sci. Eng., A, 2007, 443, 156-166.
119. B. Wilshire: Metall. Mater. Trans. A, 2002, 33, 241-248.
120. H. J. A. Frost, M. F.: 'Deformation-Mechanism Maps'; 1982, Pergamon Press.
121. F. C. Monkman and N. J. Grant: Proceedings of the American Society of Testing and Materials, 1956, 56, 593-620.
122. S. B. Brown, K. H. Kim, and L. Anand: Int. J. Plast, 1989, 5, 95-130.
123. I. S. Servi and N. J. Grant: J. Inst. Met., 1951, 80, 33-37.
124. P. J. Wray: J. Appl. Phys., 1969, 40, 4018-4029.
125. M. Ohmori, Y. Yoshinaga, and H. Maniwa: J. Jpn. Inst. Met., 1970, 8, 791-797.
126. M. Ohmori, K. Wakasa, and Y. Yoshinaga: J. Jpn. Inst. Met., 1973, 37, 1188-1194.
127. M. Ohmori, Y. Sakakibara, K. Kaneko, and Y. Yoshinaga: J. Jpn. Inst. Met., 1976, 40, 802-807.
128. N. Igata, K. Miyahara, and K. Tanaka: Trans. Jap. Inst. Met., 1979, 20, 344-346.
129. L. Felberbaum: 'Microstructure and Embrittlement of Leaded Copper Alloys', PhD thesis, Ecole Polytechnique Fédérale de Lausanne, EPFL, Lausanne, 2005.
130. R. D. K. Misra and V. S. Prasad: J. Mater. Sci., 2000, 35, 3321-3325.
131. H. Nathani and R. D. K. Misra: Mater. Sci. Technol., 2004, 20, 546-549.

132. O. D. Sherby and P. M. Burke: Prog. Mater Sci., 1967, 13, 325-390.
133. F. A. Mohamed: Mater. Sci. Eng., 1979, 40, 101-104.
134. R. P. Carreker Jr. and W. R. Hibbard Jr.: Acta Metall., 1953, 1, 655-663.
135. I. J. Spark and D. M. R. Taplin: J. Aust. Inst. Met., 1969, 14.
136. A. S. Wagh and L. N. Ezegbunam: Scr. Metall., 1984, 18, 935-937.
137. L. Orman and J. Gryziecki: Metal. Odl., 1987, 13, 361-373.
138. G. Nelmes and B. Wilshire: Scr. Metall., 1976, 10, 697-700.
139. P. C. J. Gallagher: Metall. Trans., 1970, 1, 2429-2461.
140. L. E. Murr: 'Interfacial fee energies in solid metals and alloys', in 'Interfacial Phenomena in Metals and Alloys', 142-153, 1975, Reading MA, USA, Addison-Wesley.
141. W. J. Evans and B. Wilshire: Met. Sci. J., 1970, 4, 89-94.
142. F. A. Mohamed and T. G. Langdon: Acta Metall., 1974, 22, 779-788.
143. T. Shibayanagi, S. Saji, and S. Hori: Supplement to Transactions of the Japan Institute of Metals, 1986, 27, 943-950.
144. S. Onaka, F. Tajima, S. Hashimoto, and S. Miura: Acta Metall. Mater., 1995, 43, 307-311.
145. W. Ozgowicz and M. Biscondi: J. Phys. IV, 1995, 5, 315-320.
146. J. P. Chubb and J. Billingham: Met. Technol., 1978, 5, 100-103.
147. D. J. Srolovitz, W. H. Yang, R. Najafabadi, H. Y. Wang, and R. LeSar: 'Microstructural and segregation effects in the fracture of polycrystals', in 'Materials Interfaces - Atomic-level structure and properties', (ed. D. Wolf and S. Yip), 691-702; 1992, London (UK), Chapman & Hall.
148. H. Yamagata and O. Izumi: J. Jpn. Inst. Met., 1979, 43, 209-216.
149. S. Kuramoto, Y. Nakamura, and M. Kanno: 'Effect of Zinc Addition and Melting Atmosphere on the Intermediate Temperature Embrittlement of Pure Copper', EPD Congress 1998, San Antonio, Texas, 1998, The Minerals, Metals & Materials Society, 1998, 945-956.
150. R. Nowosielski: J. Mater. Process. Technol., 2001, 109, 142-153.
151. H. Miura, T. Sakai, T. Otsuka, R. Monzen, and S. Onaka: Acta Mater., 2000, 48, 1959-1966.
152. N. I. Novokhatskaya, A. V. Serebryakov, and I. D. Chashechkin: Phys. Met., 1982, 4, 1108-1114.
153. S. Onaka, M. Kato, and R. Tanaka: Trans. Jap. Inst. Met., 1987, 28, 32-40.
154. H. Sato, T. Fujii, S. Onaka, and M. Kato: J. Mater. Sci., 2003, 38, 1689-1693.
155. S. Onaka, S. Soeta, M. Kato, and R. Tanaka: J. Mater. Sci., 1988, 23, 577-582.
156. H. Miura, T. Sakai, N. Tada, M. Kato, and T. Mori: Acta Metall. Mater., 1993, 41, 1207-1213.
157. H. Miura and T. Sakai: J. Jpn. Inst. Met., 1994, 58, 1349-1354.
158. H. Miura, T. Sakai, and M. Kato: Mater. Sci. Technol., 1994, 10, 1044-1049.
159. H. Miura and T. Sakai: J. Mater. Res., 1998, 13, 3100-3105.
160. H. Miura, T. Sakai, and H. Toda: Acta Mater., 2003, 51, 4707-4717.
161. P. Lagarde and M. Biscondi: Mem. Et. Sci. Rev. Metall., 1974, 71, 121-131.
162. R. D. Doherty, D. A. Hughes, F. J. Humphreys, J. J. Jonas, D. J. Jensen, M. E. Kassner, W. E. King, T. R. McNelley, H. J. McQueen, and A. D. Rollett: Mater. Sci. Eng., A, 1997, 238, 219-274.
163. G. Gottstein and L. S. Shvindlerman: 'Drag effects by second-phase particles', in 'Grain boundary migration in metals', (ed. B. Ralph), 150-157; 1999, CRC Press LLC.
164. S. W. Husain, M. Ahmed, and P. C. Clapp: J. Mater. Sci., 1988, 23, 1030-1035.
165. S. W. Husain and P. C. Clapp: J. Mater. Sci., 1987, 22, 2351-2356.
166. S. W. Husain and P. C. Clapp: J. Mater. Sci., 1987, 22, 509-516.
167. S. W. Husain and P. C. Clapp: Metall. Trans. A, 1988, 19, 1761-1766.
168. S. Miyazaki, T. Kawai, and K. Otsuka: Scr. Metall., 1982, 16, 431-436.

169. M. Suezawa and K. Sumino: Scr. Metall., 1976, 10, 789-792.
170. O. Izumi and Y. Harada: Trans. Jap. Inst. Met., 1970, 11, 292-299.
171. H. Yamagata and O. Izumi: J. Jpn. Inst. Met., 1978, 42, 1167-1173.
172. A. Muto, S. Goto, M. Tagami, and S. Aso: J. Jpn. Inst. Met., 1994, 58, 146-153.
173. A. Muto, S. Kawagishi, and M. Tagami: J. Jpn. Inst. Met., 1999, 63, 1062-1068.
174. W. Ozgowicz and M. Biscondi: Mem. Et. Sci. Rev. Metall., 1987, 84, 129-138.
175. M. Kanno, N. Shimodaira, T. Ohsako, and H. Suzuki: Trans. Jap. Inst. Met., 1987, 28, 73-80.
176. R. W. Evans and F. L. Jones: Met. Technol., 1978, 5, 1-6.
177. R. Nowosielski, P. Sakiewicz, and P. Gramatyka: J. Mater. Process. Technol., 2005, 162-163, 379-384.
178. Z. Sun, C. Laitem, and A. Vincent: Mater. Sci. Eng., A, 2008, 477, 145-152.
179. H. Miura, T. Sakai, N. Tada, M. Kato, and T. Mori: Scr. Metall. Mater., 1995, 32, 185-190.
180. H. Miura, H. Tamura, and T. Sakai: Scr. Mater., 1996, 34, 1871-1875.
181. T. Shibayanagi, O. Yamamoto, and S. Hori: Mater. Trans., JIM, 1990, 31, 225-227.
182. A. Muto, S. Goto, M. Tagami, and S. Aso: J. Jpn. Inst. Met., 1995, 59, 23-30.
183. F. L. Jones: Mater. Sci. Technol., 1988, 4, 256-260.
184. G. X. Wang: Acta Metall. Mater., 1994, 42, 2547-2554.
185. S. Fujiwara and K. Abiko: J. Phys. IV, 1995, 5, 295-300.
186. H. Suzuki and G. Itoh: J. Jpn. Inst. Met., 1984, 48, 1016-1021.
187. G. Gottstein and L. S. Shvindlerman: 'Drag effects during grain boundary motion', in 'Grain boundary migration in metals', (ed. B. Ralph), 133-144; 1999, CRC Press LLC.
188. E. P. George and R. L. Kennedy: 'Trace Element Effects on High Temperature Fracture', in 'Impurities in engineering materials: impact, reliability, and control', (ed. C. L. Briant), 1999, New York, Dekker.
189. C. L. Briant: Metall. Trans. A, 1990, 21, 2339-2354.
190. C. L. Briant: Mater. Sci. Technol., 2001, 17, 1317-1323.
191. C. L. Briant and S. K. Banerji: Int. Met. Rev., 1978, 23, 164-199.
192. C. L. Briant and R. P. Messmer: 'Chemical Bonding and Grain Boundary Embrittlement', Embrittlement by Liquid Metals, Watervliet NY, 1982, TMS Warrendale, PA, publ. 1983, 79-103.
193. G. Saindrenan, R. Le Gall, and F. Christien: 'Conséquences de la modification de cohésion interfaciale', in 'Endommagement interfacial des métaux', (ed. TECHNOSUP), 202-220; 2002, Paris, Ellipses édition.
194. J. R. Rice and J.-C. Wang: Mater. Sci. Eng., A, 1989, 107, 23-40.
195. M. P. Seah: Surf. Sci., 1975, 53, 168-212.
196. M. P. Seah: Acta Metall., 1980, 28, 955-962.
197. M. P. Seah and E. D. Hondros: Metall. Met. Form., 1972, 39, 100-103.
198. T. H. Courtney: 'Mechanical Behavior of Materials', 502-561; 1990, New York, NY, Mc Graw-Hill.
199. E. D. Hondros, M. P. Seah, S. Hofmann, and P. Lejcek: 'Chapter 13 - Interfacial and surface microchemistry', in 'Physical Metallurgy 4th, revised and enhanced edition', (ed. R. W. Cahn and P. Haasen), 1201-1289; 1996, Amsterdam (NL), North-Holland.
200. J. H. Westbrook: Metall. Rev., 1964, 9, 415-471.
201. G. Gottstein and L. S. Shvindlerman: 'Grain boundary migration in metals', 383; 1999, CRC Press LLC.
202. J. P. Hirth and J. R. Rice: Metall. Trans. A, 1980, 11, 1501-1511.
203. E. D. Hondros and M. P. Seah: Int. Met. Rev., 1977262-300.
204. P. Lejcek, S. Hofmann, and A. Krajnikov: Mater. Sci. Eng., A, 1997, 234-236, 283-286.

205. C. H. P. Lupis: 'Chemical Thermodynamics of Materials', 375-380; 1983, New York, Amsterdam, North-Holland, Elsevier.
206. E. V. Barrera, M. Menyhard, D. Bika, B. Rothman, and C. J. McMahon Jr.: Scr. Metall. Mater., 1992, 27, 205-210.
207. R. D. K. Misra, C. J. McMahon Jr., and A. Guha: Scr. Mater., 1994, 31, 1471-1474.
208. R. C. Muthiah, J. A. Pfaendtner, S. Ishikawa, and C. J. McMahon Jr.: Acta Mater., 1999, 47, 2797-2808.
209. J. A. Pfaendtner, R. C. Muthiah, C. T. Liu, and C. J. McMahon Jr.: Mater. Sci. Eng., A, 1999, 260, 1-11.
210. R. D. K. Misra and B. P. Kashyap: Scr. Mater., 1996, 35, 755-760.
211. R. D. K. Misra: Acta Mater., 1996, 44, 885-890.
212. A. H. Cottrell: Mater. Sci. Technol., 1990, 6, 325-329.
213. A. H. Cottrell: Mater. Sci. Technol., 1990, 6, 807-810.
214. R. Schweinfest, A. T. Paxton, and M. W. Finnis: Nature, 2004, 432, 1008-1011.
215. A. Y. Lozovoi, A. T. Paxton, and M. W. Finnis: Phys. Rev. B: Condens. Matter, 2006, 74, 155416-155411-155416-155413.
216. G. Duscher, M. F. Chisholm, U. Alber, and M. Ruhle: Nat. Mater., 2004, 3, 621-626.
217. G. A. Lopez, W. Gust, and E. J. Mittemeijer: Scr. Mater., 2003, 49, 747-753.
218. M. C. Inman, D. Mclean, and H. R. Tipler: Proc. R. Soc. London, Ser. A, 1963, 273, 538-557.
219. S. Hofmann and P. Lejcek: Interface Sci., 1996, 3, 241-267.
220. E. Voce and A. P. C. Hallowes: J. Inst. Met., 1947, 73, 323-376.
221. A. P. C. Hallowes: J. Inst. Met., 1949, 75, 839-853.
222. B. D. Powell and H. Mykura: Acta Metall., 1973, 21, 1151-1156.
223. E. D. Hondros and D. McLean: Philos. Mag. A, 1974, 29, 771-795.
224. B. D. Powell and D. P. Woodruff: Philos. Mag., 1976, 34, 169-176.
225. A. M. Donald and A. J. Craven: Philos. Mag. A, 1979, 39, 1-11.
226. J. R. Michael and D. B. Williams: Metall. Mater. Trans. A, 1984, 15, 99-105.
227. J. D. Russell and A. T. Winter: Scr. Metall., 1985, 19, 575-579.
228. M. Menyhard, B. Blum, and C. J. McMahon Jr.: Acta Metall. Mater., 1989, 37, 549-557.
229. Z.-Q. Li, G.-H. Li, Y. Qin, H. Shen, and X.-J. Wu: Scr. Metall. Mater., 1991, 25, 367-370.
230. Z.-Q. Li, G.-H. Li, H. Shen, Y. Qin, X.-J. Wu, and D.-X. Peng: Mater. Sci. Eng., A, 1993, 163, 73-79.
231. G. H. Li and L. D. Zhang: Scr. Metall. Mater., 1995, 32, 1335-1340.
232. V. J. Keast, J. Bruley, P. Rez, J. M. Maclaren, and D. B. Williams: Acta Mater., 1998, 46, 481-490.
233. J. Bruley, V. J. Keast, and D. B. Williams: Acta Mater., 1999, 47, 4009-4017.
234. U. Alber, H. Mullejans, and M. Ruhle: Acta Mater., 1999, 47, 4047-4060.
235. R. Monzen, T. Kuze, T. Okamoto, and H. Miura: Metall. Mater. Trans. A, 1999, 30, 483-485.
236. V. J. Keast and D. B. Williams: Acta Mater., 1999, 47, 3999-4008.
237. L.-S. Chang, E. Rabkin, S. Hofmann, and W. Gust: Acta Mater., 1999, 47, 2951-2959.
238. L.-S. Chang, E. Rabkin, B. B. Straumal, B. Baretzky, and W. Gust: Acta Mater., 1999, 47, 4041-4046.
239. W. Sigle, L.-S. Chang, and W. Gust: Philos. Mag. A, 2002, 82, 1595-1608.
240. L. S. Chang, B. Straumal, E. Rabkin, W. Lojkowski, and W. Gust: Acta Mater., 2007, 55, 335-343.
241. S. Divinski, M. Lohmann, C. Herzig, B. Straumal, B. Baretzky, and W. Gust: Phys. Rev. B: Condens. Matter, 2005, 71, 104104-104101-104104-104108.
242. A. Joshi and D. F. Stein: J. Inst. Met., 1971, 99, 178-181.
243. J. T. Plewes: Adv. Mater. Processes, 1991, 10, 23-27.

244. H. L. Marcus and N. E. Paton: Metall. Trans., 1974, 5, 2135-2138.
245. D. J. Hunt, D. T. Peters, and J. W. Wilson: Applic. Surf. Sci., 1981, 9, 141-164.
246. M. J. Saarivirta: Trans. ASM, 1964, 57, 133-141.
247. S. P. Clough and D. F. Stein: Scr. Metall., 1975, 9, 1163-1166.
248. A. Pineau, B. Aufray, F. Cabane-Brouty, and J. Cabane: Acta Metall., 1983, 31, 1047-1052.
249. R. D. K. Misra, V. S. Prasad, and P. R. Rao: Scr. Mater., 1996, 35, 129-133.
250. H. J. McQueen and N. D. Ryan: Mater. Sci. Eng., A, 2002, 322, 43-63.
251. H. R. Tipler and D. McLean: Met. Sci. J., 1970, 4, 103-107.
252. T. G. Nieh and W. D. Nix: Metall. Trans. A, 1981, 12, 893-901.
253. D. McLean: J. Inst. Met., 1952, 81, 121-123.
254. R. Monzen, O. Matsuda, and H. Miura: Z. Metall., 2002, 93, 840-844.
255. B. S. Bokstein and A. N. Smimov: Mater. Lett., 2003, 57, 4501-4504.
256. J. K. O. Asante, W. D. Roos, and J. J. Terblans: Surf. Interface Anal., 2003, 35, 441-444.
257. R. Monzen, T. Kuze, O. Matsuda, and H. Miura: Metall. Mater. Trans. A, 2003, 34, 773-779.
258. R. Monzen, O. Matsuda, and H. Miura: Mater. Sci. Eng., A, 2004, 387-89, 424-427.
259. M. Sanchez Medina, R. Sangiorgi, and N. Eustathopoulos: Scr. Mater., 1981, 15, 737-738.
260. R. Eborall and P. Gregory: J. Inst. Met., 1955, 84, 88-90.
261. R. P. Messmer and C. L. Briant: Acta Metall., 1982, 30, 457-467.
262. S. Han, S. Kim, M. Kong, and C. Kim: Metall. Mater. Trans. A, 2002, 33, 3298-3300.
263. X. Y. Liu, W. Kane, and C. J. McMahon Jr.: Scr. Mater., 2004, 50, 673-677.
264. R. J. Jackson, D. A. Edge, and D. C. Moore: J. Inst. Met., 1970, 98, 160-165.
265. M. Kanno and N. Shimodaira: Scr. Mater., 1987, 21, 1487-1492.
266. M. Kanno and N. Shimodaira: Trans. Jap. Inst. Met., 1987, 28, 742-748.
267. S. V. Shevchenko, I. M. Neklyudov, A. T. Lopata, V. N. Voevodin, and V. I. Sytin: Mater. Sci., 2000, 36, 901-909.
268. W. A. Baker and A. P. C. Hallowes: J. Inst. Met., 1949, 75, 741-758.
269. K. Kubosono, I. Asamizu, M. Iwase, and T. Kurita: Copper-Nickel Based Alloy, 1995, US Patent n° 5,441,696.
270. P. A. Korzhavyi, I. A. Abrikosov, and B. Johansson: Acta Mater., 1999, 47, 1417-1424.
271. A. Jablonski and C. J. Powell: Surf. Interface Anal., 1993, 20, 771-786.
272. C. Linsmeier: Vacuum, 1994, 45, 673-690.
273. M. P. Seah and I. S. Gilmore: Surf. Interface Anal., 1998, 26, 908-929.
274. M. P. Seah: Appl. Surf. Sci., 1999, 144-145, 161-167.
275. M. P. Seah: J. Electron. Spectrosc. Relat. Phenom., 1999, 100, 55-73.
276. D. T. L. Van Agterveld, G. Palasantzas, and J. T. M. De Hosson: Acta Mater., 2000, 48, 1995-2004.
277. V. Laporte, P. Berger, and K. Wolski: Surf. Interface Anal., 2005, 37, 809-820.
278. D. Mclean: 'Grain boundaries in metals'; 1957, Oxford Univ. Press.
279. V. J. Keast and D. B. Williams: Curr. Opin. Solid State Mater. Sci., 2001, 5, 23-30.
280. H. Kokawa, T. Watanabe, and S. Karashima: Philos. Mag. A, 1981, 44, 1239-1254.
281. T. Watanabe, S. Tsurekawa, S. Kobayashi, and S.-I. Yamaura: Mater. Sci. Eng., A, 2005, 410-411, 140-147.
282. H. Miura and T. Sakai: Scr. Metall. Mater., 1995, 32, 1753-1758.
283. H. Miura, N. Tada, T. Sakai, and M. Kato: Mater. Sci. Forum, 1996, 207-209, 649-652.
284. H. Miura, S. Watanabe, and T. Sakai: Interface Sci., 1997, 4, 329-338.
285. P. A. Thorsen and J. B. Bilde-Sorensen: Mater. Sci. Forum, 1999, 294-296, 131-134.
286. A. L. Pinto, C. S. D. Viana, and L. H. de Almeida: Mater. Sci. Eng., A, 2007, 445, 14-19.
287. H. Davies and V. Randle: Mater. Sci. Technol., 2000, 16, 1399-1402.

288. H. Davies and V. Randle: Philos. Mag. A, 2001, 81, 2553-2564.
289. V. Randle and H. Davies: Metall. Mater. Trans. A, 2002, 33, 1853-1857.
290. G. S. Rohrer, V. Randle, C. S. Kim, and Y. Hu: Acta Mater., 2006, 54, 4489-4502.
291. S. Y. Lee, Y. B. Chun, J. W. Han, and S. K. Hwang: Mater. Sci. Eng., A, 2003, 363, 307-315.
292. W. E. King and A. J. Schwartz: Scr. Mater., 1998, 38, 449-455.
293. M. Kumar, A. J. Schwartz, and W. E. King: Acta Mater., 2002, 50, 2599-2612.
294. M. Kumar, W. E. King, and A. J. Schwartz: Acta Mater., 2000, 48, 2081-2091.
295. A. J. Schwartz and W. E. King: J. Min. Met. Mater. Soc., 1998, 50, 50-55.
296. V. Randle, Y. Hu, and M. Coleman: J. Mater. Sci., 2008, 43, 3782-3791.
297. V. Randle, G. S. Rohrer, H. M. Miller, M. Coleman, and G. T. Owen: Acta Mater., 2008, 56, 2363-2373.
298. M. G. Nicholas: 'A Survey of Litterature on Liquid Metal Embrittlement of metals and Alloys', Embrittlement by Liquid and Solid Metals, St.-Louis, Missouri, 1982, The Metallurgical Society of AIME, 27-50.
299. W. Rostoker: 'Liquid Metal Embrittlement', in 'Metals Handbook, Desk Edition', (ed. H. E. Boyer and T. L. Gall), 32.26-32.27; 1985, Metals Park, OH, American Society for Metals.
300. M. H. Kamdar: Prog. Mater Sci., 1973, 15, 289-374.
301. M. G. Nicholas and C. F. Old: J. Mater. Sci., 1979, 14, 1-18.
302. N. S. Stoloff: 'Metal Induced Embrittlement - A Historical Perspective', Embrittlement by Liquid and Solid Metals, St.-Louis, Missouri, 1982, The Metallurgical Society of AIME, 3-26.
303. J. R. Pickens and A. R. C. Westwood: 'Recent Soviet Contributions to the Understanding and Application of Liquid Metal Induced Embrittlement Phenomena', Embrittlement by Liquid and Solid Metals, St.-Louis, Missouri, 1982, The Metallurgical Society of AIME, 51-64.
304. S. P. Lynch: Acta Metall., 1988, 36, 2639-2661.
305. S. P. Lynch: Mater. Charact., 1992, 28, 279-289.
306. P. J. L. Fernandes, R. E. Clegg, and D. R. H. Jones: Eng. Fail. Anal., 1994, 1, 51-63.
307. P. J. L. Fernandes and D. R. H. Jones: Int. Mater. Rev., 1997, 42, 251-261.
308. B. Joseph, M. Picat, and F. Barbier: Eur. Phys. J. Appl. Phys., 1999, 5, 19-31.
309. S. P. Lynch: J. Fail. Anal. Prev., 2008, 8, 259-274.
310. P. J. L. Fernandes and D. R. H. Jones: Eng. Fail. Anal., 1996, 3, 299-302.
311. J. A. Pfaendtner and C. J. McMahon Jr.: Acta Mater., 2001, 49, 3369-3377.
312. S. W. Woods and J. McMahon, C. J.: Scr. Mater., 2001, 45, 1307-1311.
313. R. Muthiah, A. Guha, and C. J. McMahon Jr.: Mater. Sci. Forum, 1996, 207-209.
314. D. Bika and C. J. McMahon Jr.: Acta Metall. Mater., 1995, 43, 1909-1916.
315. W. M. Kane, U. Krupp, T. Jacobs, and C. J. McMahon Jr.: Mater. Sci. Eng., A, 2005, 402, 42-46.
316. U. Krupp, W. M. Kane, C. Laird, and C. J. McMahon Jr.: Mater. Sci. Eng., A, 2004, 387-89, 409-413.
317. U. Krupp and C. J. Mcmahon Jr.: J. Alloys Compd., 2004, 378, 79-84.
318. U. Krupp: Int. Mater. Rev., 2005, 50, 83-97.
319. Y. Mishin, P. Sofronis, and J. L. Bassani: Acta Mater., 2002, 50, 3609-3622.
320. Y. Xu and J. L. Bassani: Mater. Sci. Eng., A, 1999, 260, 48-54.
321. C. J. McMahon Jr.: Interface Sci., 2004, 12, 141-146.
322. V. Michaud and A. Mortensen: Composites Part A, 2001, 32, 981-996.
323. W. R. Warke: 'Liquid Metal and Solid Metal Induced Embrittlement', in 'Failure Analysis and Prevention', 861-867, 2001, Materials Park, OH, USA, ASM International.

324. M. H. Kamdar: 'Liquid-Metal Embrittlement', in 'Corrosion',171-184, 2001, Materials Park, OH, USA, ASM International.
325. G. Kumar and K. N. Prabhu: Adv. Colloid Interface Sci., 2007, 133, 61-89.
326. N. Eustathopoulos, N. Sobczak, A. Passerone, and K. Nogi: J. Mater. Sci., 2005, 40, 2271-2280.
327. T. Auger, G. Lorang, S. Guerin, J.-L. Pastol, and D. Gorse: J. Nucl. Mater., 2004, 335, 227-231.
328. E. E. Glickman: 'Mechanism of Liquid Metal Embrittlement by Simple Experiments: from Atomics to Life-Time', Multiscale Phenomena in Plasticity, Ouranopolis, Greece, 2000, Kluwer Academic Publisher, 383-401.
329. P. Gordon: Metall. Trans. A, 1978, 9A, 267-273.
330. D. D. Perovic, G. C. Weatherly, and W. A. Miller: Scr. Mater., 1987, 21, 345-347.
331. R. B. Waterhouse and D. Grubb: J. Inst. Met., 1963, 91, 216-219.
332. W. L. Vasconcelos, P. R. Cetlin, and C. A. Bottrel-Coutinho: Scr. Mater., 1993, 29, 1195-1198.
333. J. V. Rinnovatore, J. D. Corrie, and H. Markus: Trans. ASM, 1964, 57, 474-481.
334. J. V. Rinnovatore, J. D. Corrie, and H. Markus: Trans. ASM, 1966, 59, 665-671.
335. J. V. Rinnovatore, J. D. Corrie, and J. D. Meakin: ASM Trans. Q., 1968, 61, 321-325.
336. R. Chadwick: J. Inst. Met., 1969, 97, 93-97.
337. C. F. Old and P. Trevena: Met. Sci., 1981, 15, 281-285.
338. J. Lerner and C. J. McMahon Jr.: Mater. Sci. Eng., A, 2002, 336, 72-74.
339. J. Lerner, S. S. Woods, E. Peng, and C. J. McMahon Jr: Mater. Sci. Eng., A, 2003, 345, 357-358.
340. E. E. Glickman: Interface Sci., 2003, 11, 451-459.
341. K. Ina and H. Koizumi: Mater. Sci. Eng., A, 2004, 387-89, 390-394.
342. K. Wolski, V. Laporte, N. Marié, and M. Biscondi: Interface Sci., 2001, 9, 183-189.
343. W. R. Warke and U. N. Nanda: J. Met., 1982, 34, 41-41.
344. A. W. Funkenbusch, L. A. Heldt, and D. F. Stein: 'Influence of Phosphorous on Intergranular Mercury and Hydrogen Embrittlement of a Nickel-Copper Alloy', Embrittlement by Liquid and Solid Metals, St.-Louis, Missouri, 1982, The Metallurgical Society of AIME, 241-251.
345. S. Kuyucak and M. Sahoo: Can. Metall. Q., 1996, 35, 1-15.
346. European Union: 'Directive 2002/96/EC on waste electrical and electronic equipment', 2002.
347. European Union: 'Directive 2002/95/EC on the restriction of the use of certain hazardous substances in electrical and electronic equipment', 2002.
348. European Union: 'Directive 2000/53/EC on End-of-Life Vehicle', 2000.
349. Environmental Protection Agency: 'National Primary Drinking Water Regulations for Lead and Copper: EPA-HQ-OW-2005-0034', 2005.
350. European Union: 'Directive 1998/83/EC on the quality of water intended for human consumption', 1998.
351. G. M. Pharr, P. S. Godavarti, and B. L. Vaandrager: J. Mater. Sci., 1989, 24, 784-792.
352. M. Sadayappan, J. P. Thomson, M. Sahoo, and H. T. Michels: 'High temperature properties of Bi-containing copper alloys for plumbing applications', Copper'06, Compiègne, 2006, Wiley-VCH, 179-184.
353. N. Eustathopoulos: Int. Met. Rev., 1983, 28, 189-210.
354. D. Chatain, E. Rabkin, J. Derenne, and J. Bernardini: Acta Mater., 2001, 49, 1123-1128.
355. T. Mori, H. Miura, T. Tokita, J. Haji, and M. Kato: Philos. Mag. Lett., 1988, 58, 11-15.
356. L. Felberbaum, A. Rossoll, and A. Mortensen: J. Mater. Sci., 2005, 40.
357. R. Raj: J. Am. Ceram. Soc., 1986, 69, 708-712.

358. J. Koike, K. Miki, H. Takahashi, and K. Maruyama: Mater. Sci. Eng., A, 2000, 285, 158-164.
359. V. Bursikova, J. Bursik, V. Navratil, and K. Milicka: Mater. Sci. Eng., A, 2002, 324, 235-238.
360. L. Felberbaum and A. Mortensen: Scr. Mater., 2006, 55, 955-958.
361. H. Miura, T. Otsuka, T. Sakai, and S. Onaka: Scr. Mater., 1999, 40, 33-38.
362. H. Miura, T. Sakai, H. Tamura, and G. Gottstein: Acta Mater., 1999, 47, 757-768.
363. L. Felberbaum, V. Laporte, and A. Mortensen: Scr. Mater., 2008, 58, 610-613.
364. E. D. Shchukin: Colloids Surf., A, 1999, 149, 529-537.
365. P. A. Rehbinder and E. D. Shchukin: Prog. Surf. Sci., 1972, 3, 97-188.
366. W. Rostoker, J. M. McHaughey, and H. Markus: 'Embrittlement by Liquid Metals'; 1960, Reinhold Publishing Corp., New-York (USA) / Chapman & Hall, London (UK).
367. S. A. Gavin, J. P. Chubb, and J. Billingham: 'Effect of Impurities on the Hot Ductility of Cupro-nickel Alloys', Proc. Conf. "Grain Boundaries", Surrey University, 1976, C25-C30.
368. J. P. Beckman and D. A. Woodford: Metall. Trans. A, 1989, 20, 184-187.

Figures:

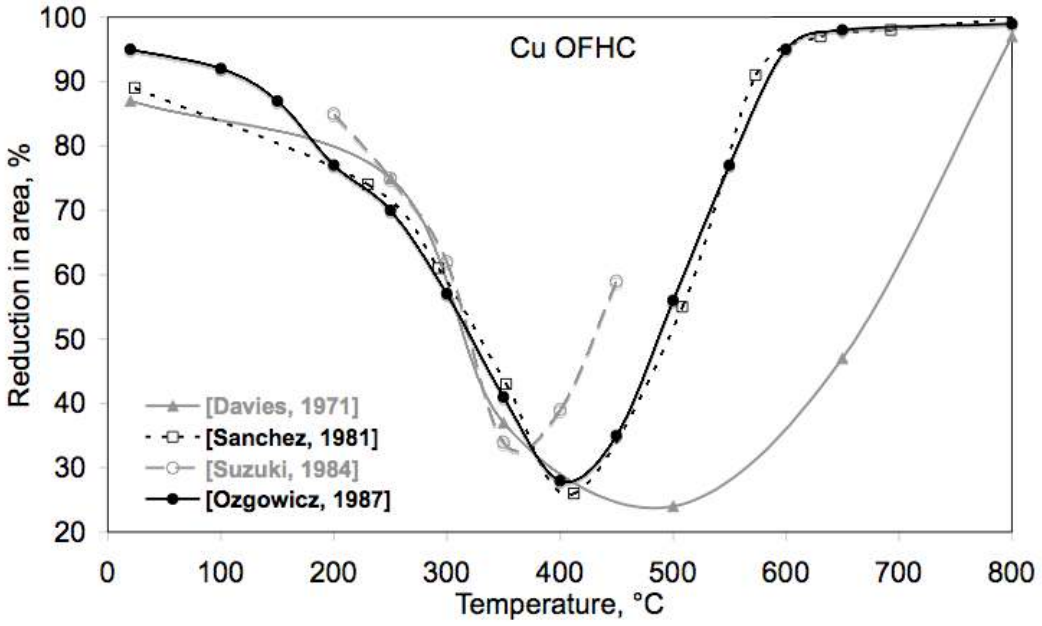

Figure 1 - Reduction in area versus deformation temperature in tensile testing of OFHC copper: empty circles from data gathered under vacuum at 4.6×10^{-4} s^{-1} on OFHC copper of average grain size 300-400 μm by Suzuki and Itoh[182]; full circles from data gathered under argon at 1×10^{-3} s^{-1} on OFHC copper of average grain size 150 μm by Ozgowicz and Biscondi[170]; empty squares from

data gathered under argon at 10^{-3} s^{-1} on OFHC copper of average grain size 150 μm by Sanchez-Medina et al.[255] and full triangles from data gathered under vacuum at roughly 10^{-3} s^{-1} on OFHC copper of average grain size 100 μm by Davies and al.[6].

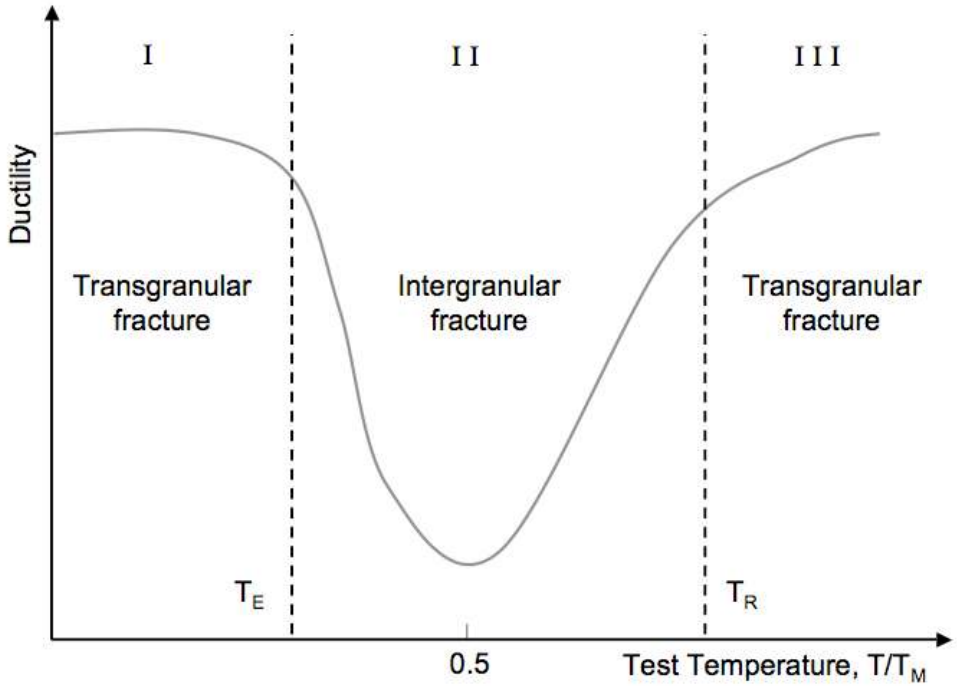

(a)

Figure 2a – General shape and features of the ductility trough (after Refs.[6, 11]);

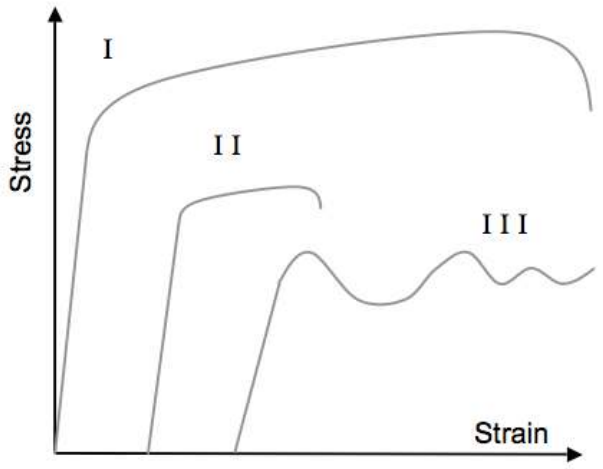

Figure 2b – Sketch of the shape of tensile curves in relation to Fig. 3a (after Refs.[6, 11]);

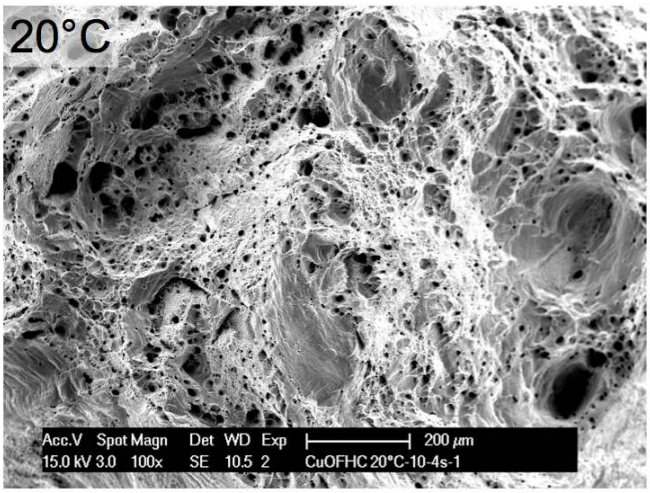

Figure 2c – Fractured surface of tensile specimens of OFHC copper tested at 20°C at a strain rate of 10^{-4} s^{-1};

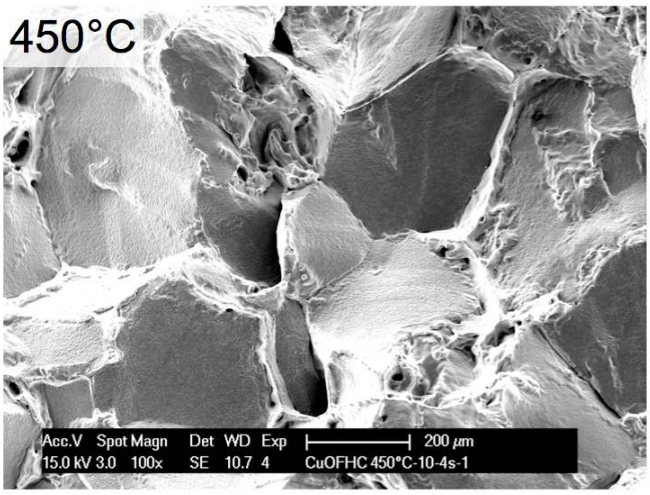

Figure 2d – Fractured surface of tensile specimens of OFHC copper tested at 450°C at a strain rate of 10^{-4} s^{-1};

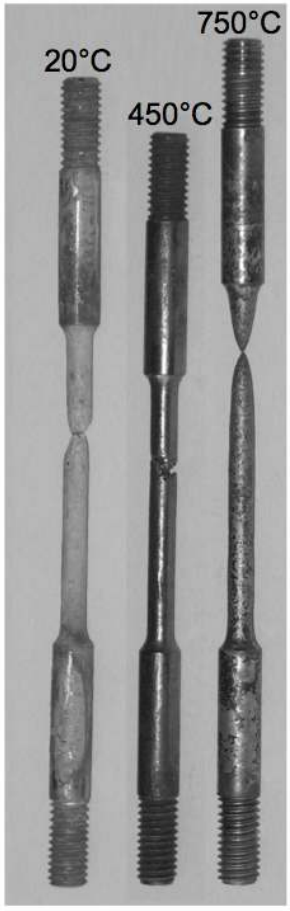

Figure 2e – Fractured tensile specimens of OFHC copper tested at a strain rate of 10^{-4} s^{-1} (round bars with a Ø4 mm initial diameter) .

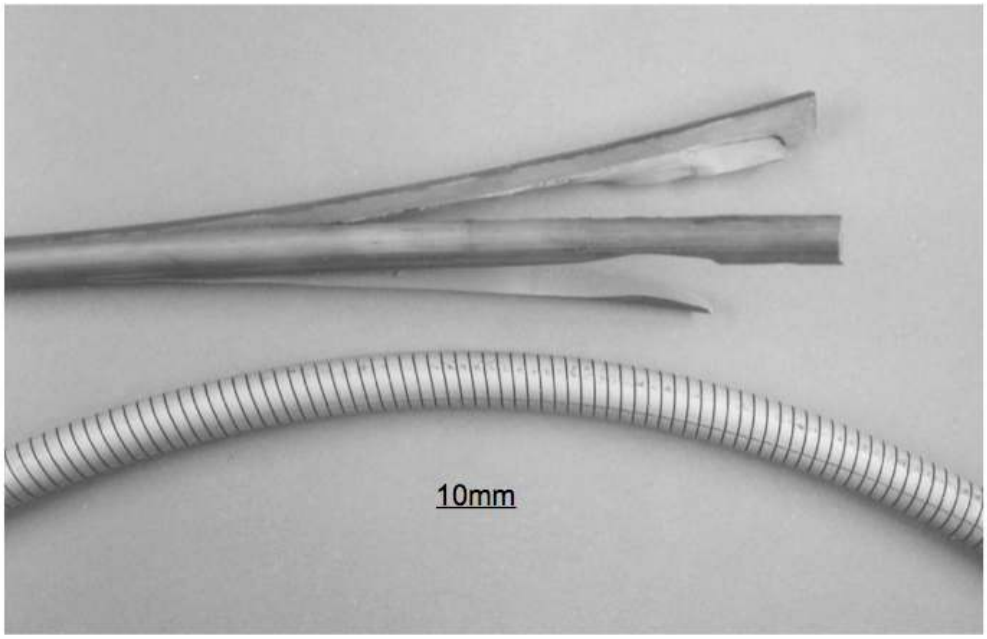

Figure 3 – Two different examples of cracks formed as a result of embrittlement of copper-nickel based alloys ; top: longitudinal cracks caused by residual stresses; bottom: spiral-shaped crack formed during extrusion (courtesy of Swissmetal®, Dornach, Switzerland).

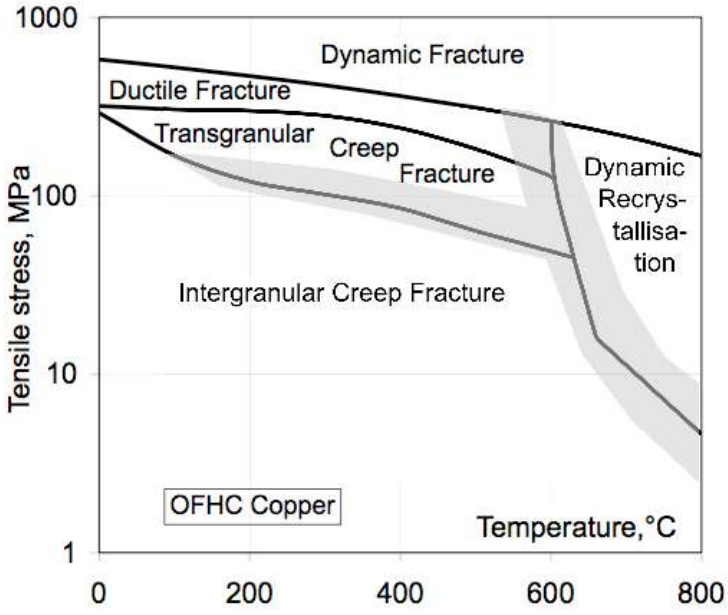

Figure 4a - The fracture mechanism map for OFHC copper (redrawn from Ref.[14]);

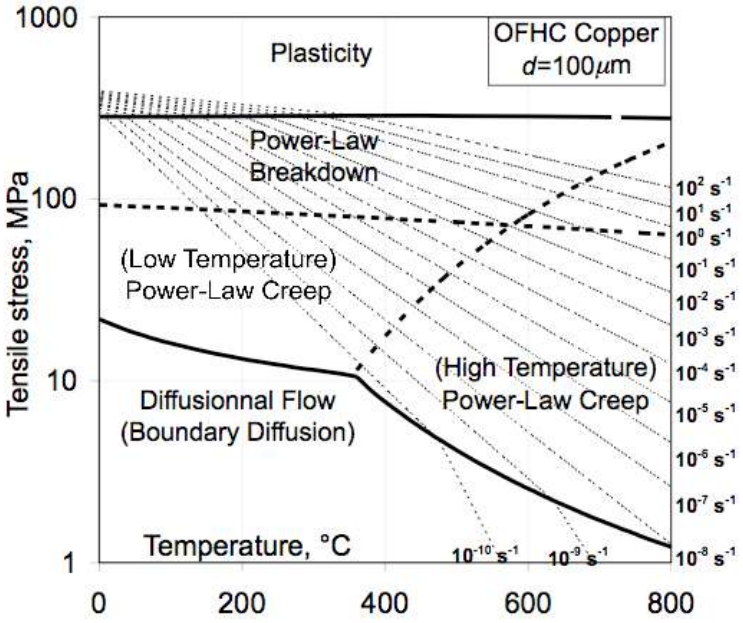

Figure 4b - The deformation mechanism map for OFHC copper (redrawn from Ref.[116]): strain rates refer to constant secondary creep rates;

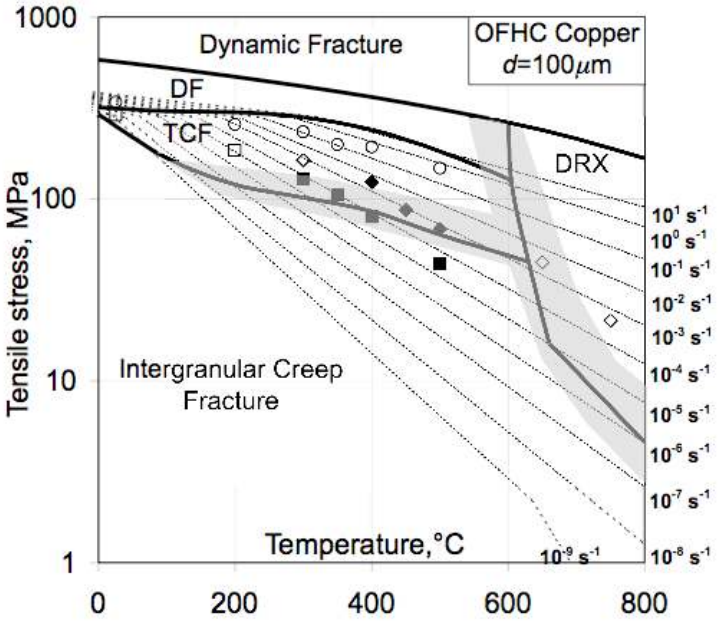

Figure 4c - Constant secondary creep rate curves (redrawn from Ref.[116]) superimposed on the fracture mechanism map (redrawn from Ref.[14]) together with experimental data points: full symbol denotes brittle intergranular fracture, empty symbols denote ductile rupture, squares from data gathered at 10^{-4} s^{-1} by Felberbaum[125] on OFHC copper of average grain size 25 μm, circles from data gathered at 10 s^{-1} by Felberbaum[125] on OFHC copper of average grain size 25 μm, diamonds from data gathered at 4.4×10^{-3} s^{-1} by Igata et al.[124] on OFHC copper of average grain size 50 μm, showing the ductility trough (with DF: Ductile Fracture, TCF: Transgranular Creep Fracture and DRX: Dynamic Recrystallisation);

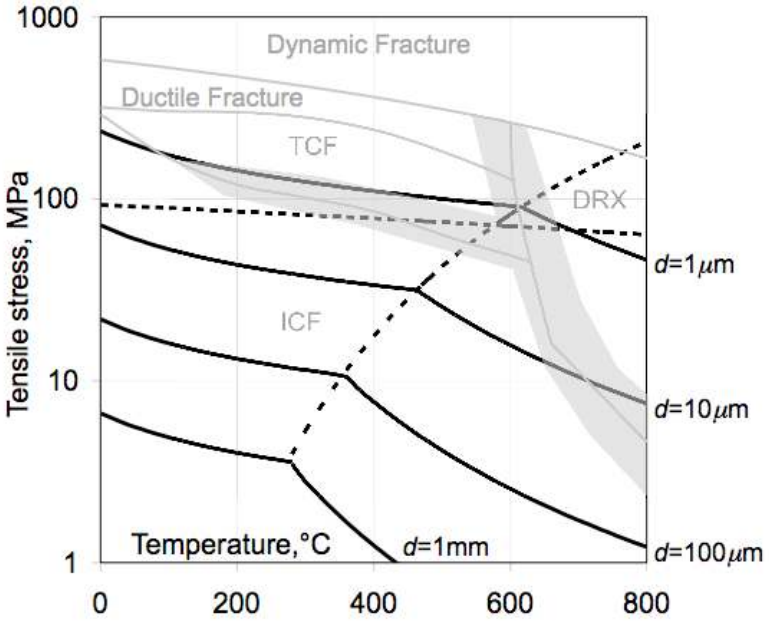

Figure 4d - The influence of grain size *d* on the transition in dominance of diffusive creep (below black lines indexed with discrete values for *d*) versus power-law creep (above previously mentioned black lines) after Ref.[116] (with ICF: Intergranular Creep Fracture). The quasi-horizontal dotted line is the low limit for Power-Law Breakdown while the other (curved) dotted line separates High and Low Temperature Power-Law creep (see Fig. 4b, which is plotted for d=100μm).

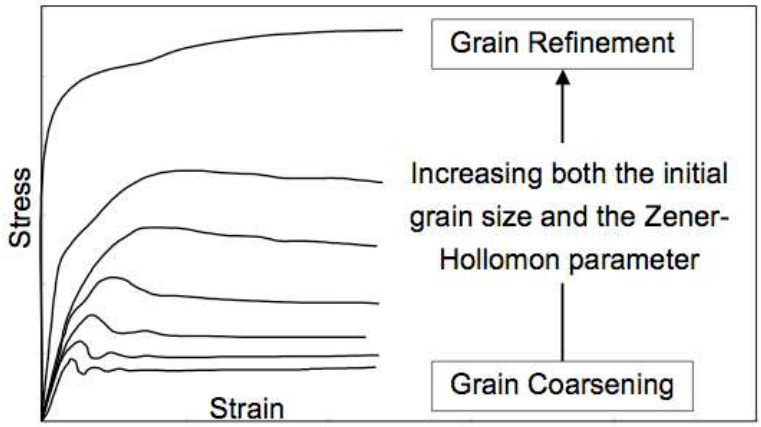

Figure 5 - Sketched flow curves in the presence of dynamic recrystallisation with an indication of the influence of the initial grain size, plus that of temperature T and strain rate combined into the Zener-Hollomon parameter , with Q, the activation energy and k, Boltzman's constant (after Sakai and Jonas[66]).

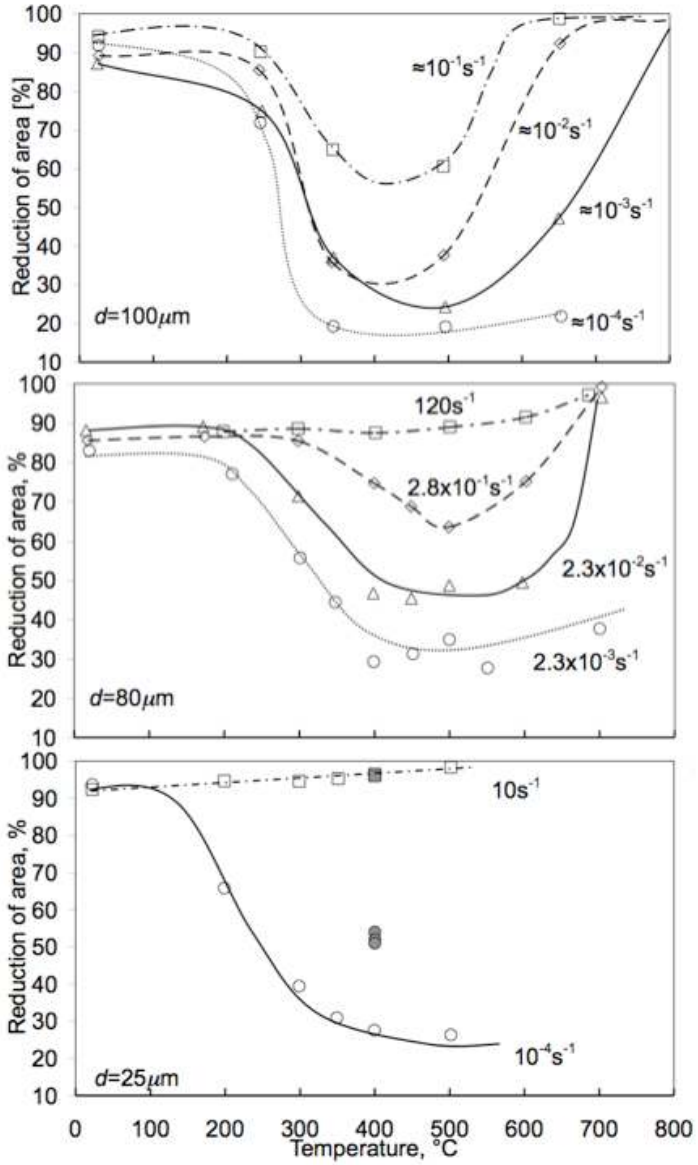

Figure 6 - Ductility trough variation as a function of strain rate. Top: after Ref.[6]; squares from data gathered at roughly 10^{-1} s^{-1}, diamonds for data gathered at roughly 10^{-2} s^{-1}, triangles for data gathered at roughly 10^{-3} s^{-1} and circles for data gathered at roughly 10^{-4} s^{-1} on OFHC copper of average grain size 100 μm). Middle graph after Ref.[123]; squares for data gathered at 120 s^{-1}, diamonds for data gathered at 2.8×10^{-1} s^{-1}, triangles for data gathered at 2.3×10^{-2} s^{-1} and circles for

data gathered at 2.3×10^{-3} s^{-1} on OFHC copper of average grain size 80 μm. Bottom: after Ref.[125]; full symbols denote 4N Copper; empty symbols denote OFHC Copper, circles for data gathered at 10^{-4} s^{-1}, squares for data gathered at 10 s^{-1} on copper of average grain size 25 μm.

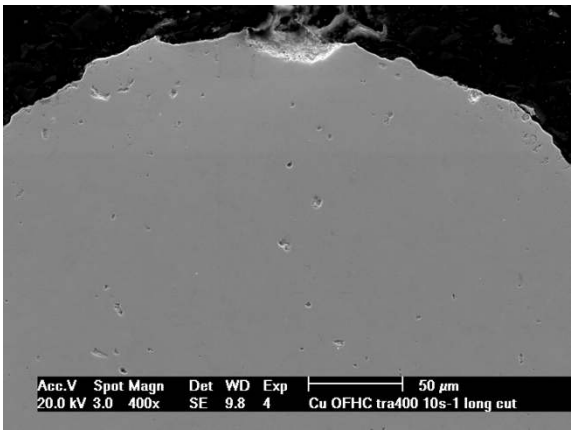

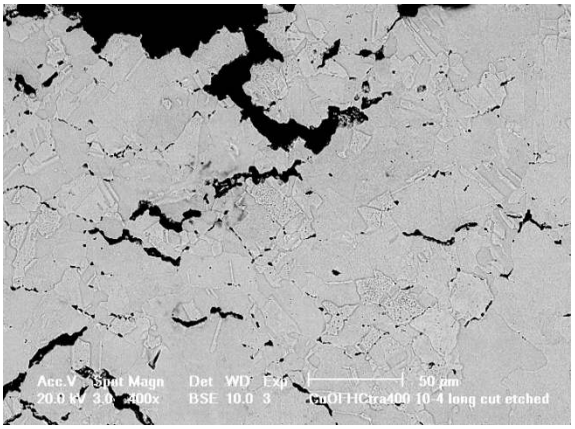

(a) CuOFHC, , *RA*=97% (b) CuOFHC, , *RA*=28%

Figure 7 - Longitudinal cuts across the tensile fracture surface of round bars of OFHC copper, tested at (a) 10 s^{-1} and (b) 10^{-4} s^{-1} (*RA* = Reduction in Area); as seen, fracture at the lower strain rate is accompanied by extensive internal damage development (from Felberbaum[125]).

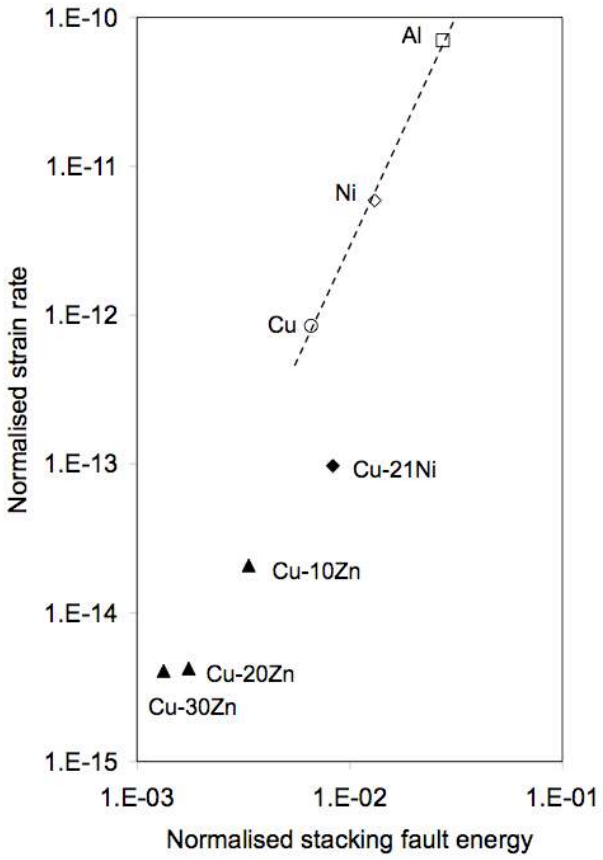

Figure 8 - Redrawn from Mohamed and Langdon[138] where the normalised creep rate is defined as (: steady state creep rate, k: Boltzman's constant, T: temperature, D: Herring-Weertman weighted diffusion coefficient, G: shear modulus and b: Burgers' vector length) and the stacking fault energy γ is normalised by Gb; data were obtained for an applied stress of $2.10^{-4} G$.

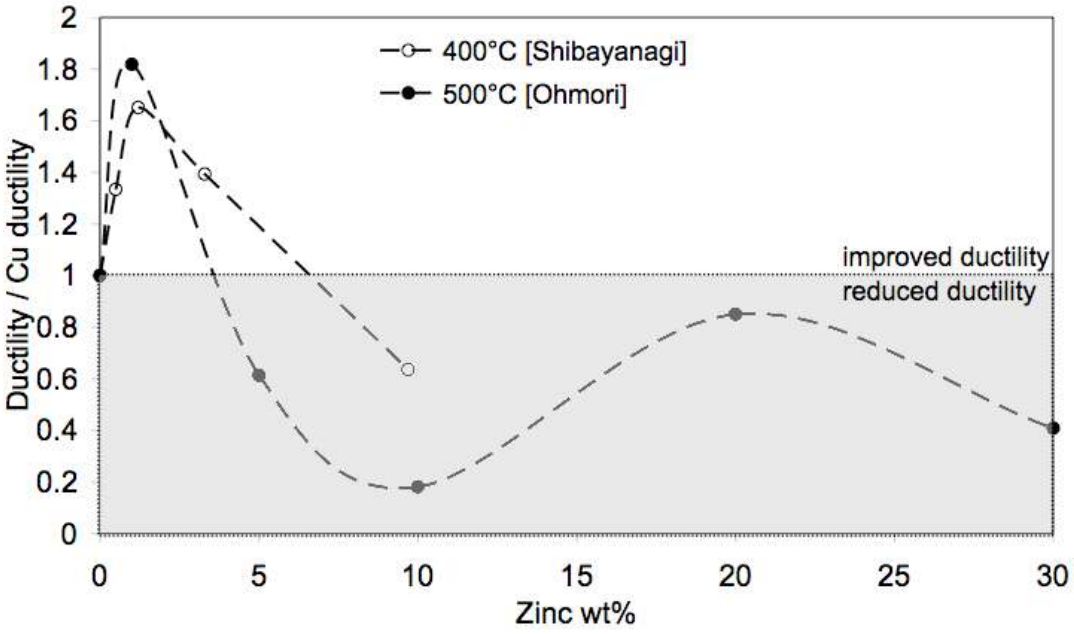

Figure 9 - Influence of zinc content on the ITE of α-brass at 400 and 500°C (after Ohmori[122, 139] and Shibayanagi[122, 139]).

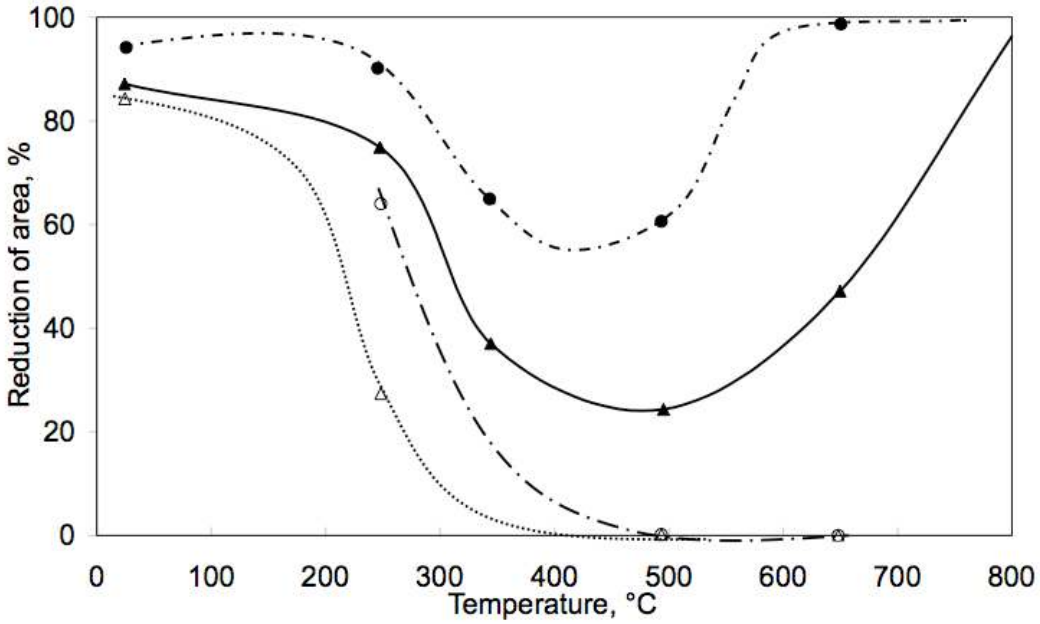

Figure 10 – Ductility trough in pure (full symbols) and internally oxidised (hollow symbols) polycrystalline copper with two different strain rate: circles are from data gathered at roughly 10^{-1} s^{-1} and triangles from data gathered at roughly 10^{-3} s^{-1}; grain size is around 100 μm (after Davies et al.[6]).

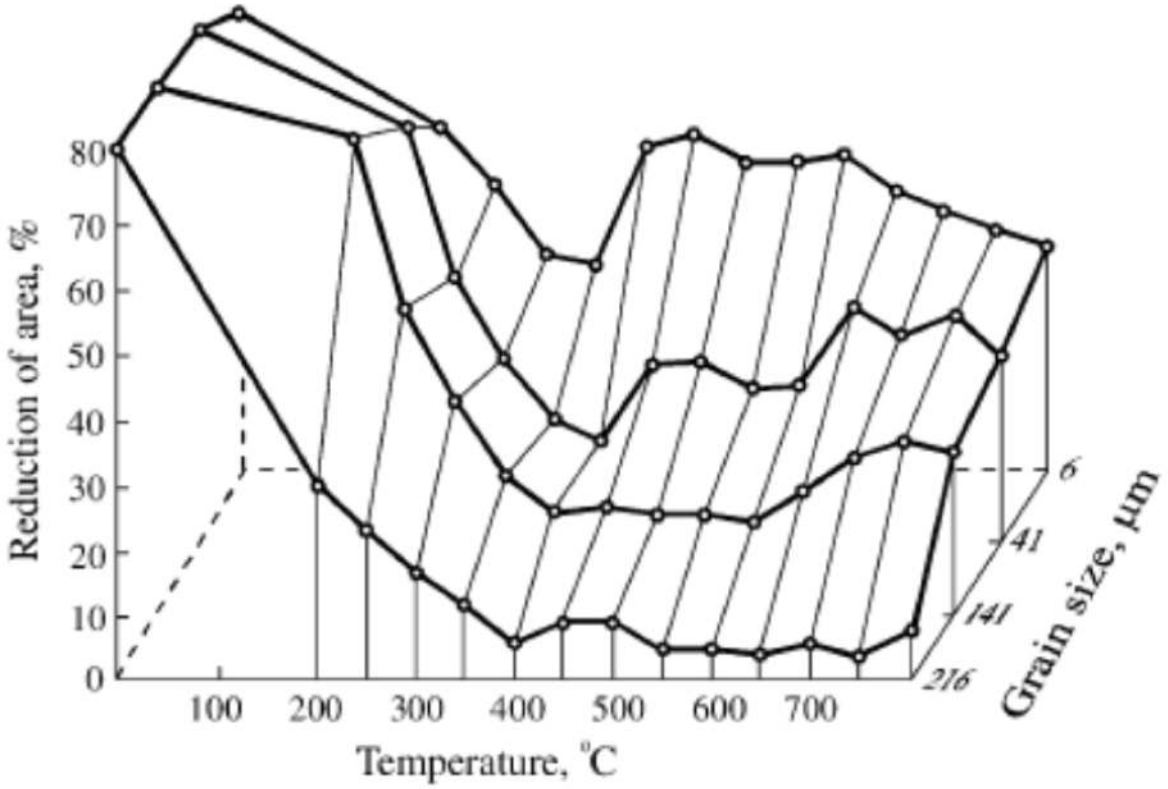

Figure 11 - Reduction in area versus deformation temperature and grain size of industrial bronze CuSn6 stretched at a strain rate of 1.19×10^{-3} s^{-1}. Figure reproduced from Ozgowicz[3], with permission from Elsevier Ltd.

Figure 12 - Ductility troughs in OFHC (Oxygen Free High Conductivity, i.e. 3N5) Copper (containing 6ppm of sulphur) and OSFC (Oxygen and Sulphur Free: sulphur concentration less than 1ppm) Copper after Suzuki[182] (tests conducted in vacuum at 4.6×10^{-4} s^{-1}), and in copper of varying purity after Fujiwara[181] (tests conducted in vacuum at 4.2×10^{-5} s^{-1}).

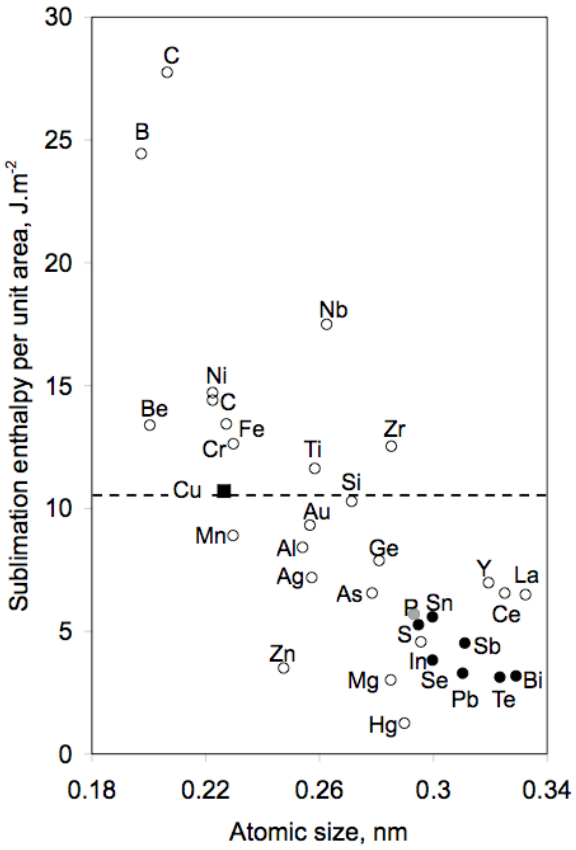

Figure 13 - Sublimation enthalpy of 33 elements redrawn from Seah[192]; full symbols are known embrittlers of copper.

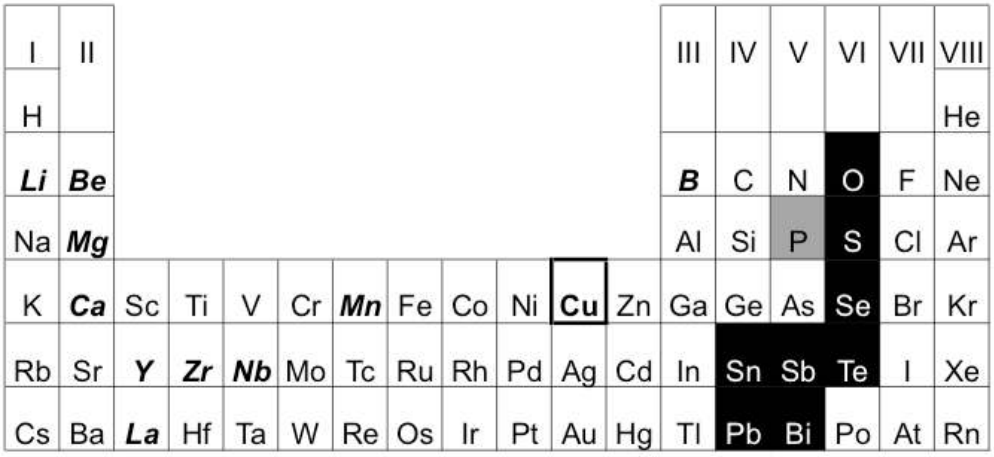

Figure 14 - Periodic table of the elements indicating in black known embrittlers of copper, and in bold-italics known “de-embrittlers” of copper.

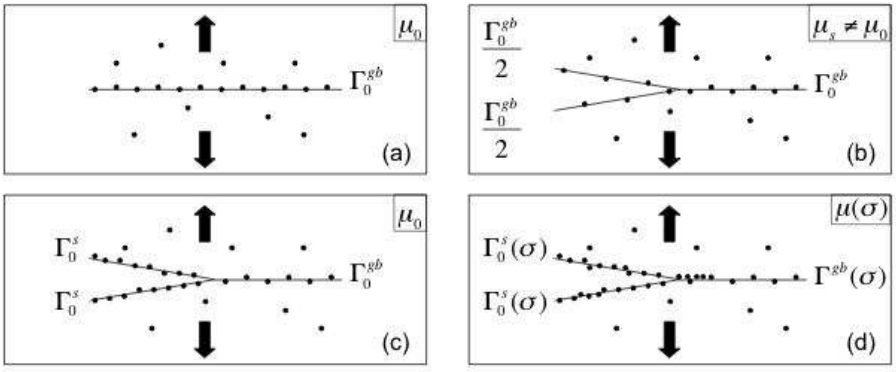

Figure 15 - (a) segregated grain boundary submitted to a tensile stress with a constant grain boundary segregant concentration Γ_0^{gb}; (b) rapid fracture of the grain boundary: the impurity global segregation level is unchanged and the segregant chemical potential μ is therefore not uniform; (c) quasistatic fracture of the grain boundary; here the free surface concentration Γ_0^{s} is dictated by equalisation of the segregant chemical activity μ across the sample; (d) dynamic embrittlement comprising diffusion-controlled stress-induced segregant concentration changes at the crack tip.

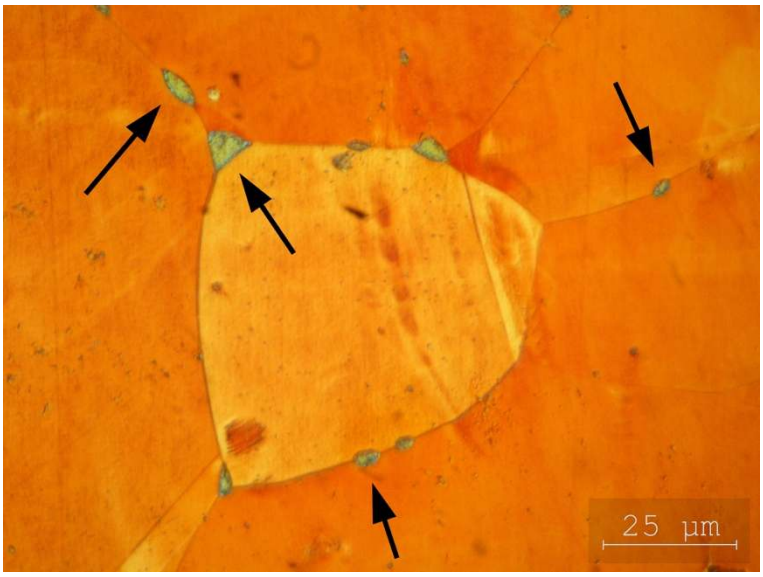

Figure 16 – Polished section of a Cu-1Pb sample heat treated at 900 °C 1 h and 400 °C 24 h; selected lead inclusions are indicated by arrows (after Felberbaum[125]).

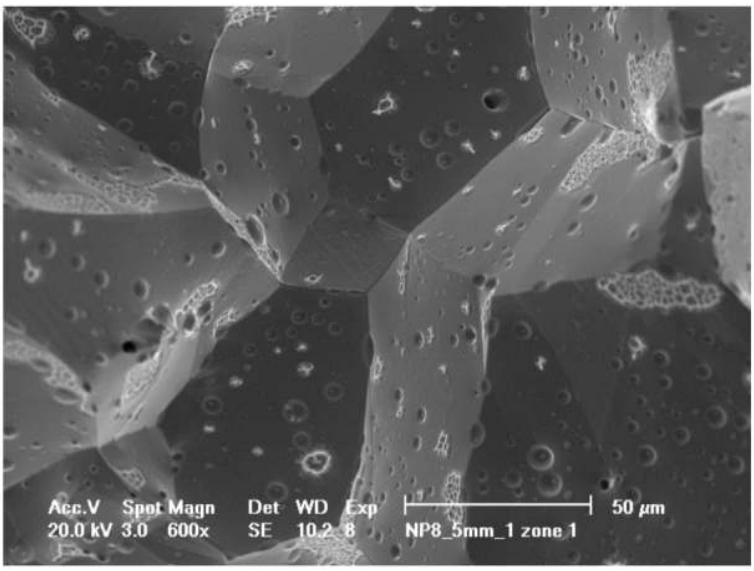

Figure 17 - Sharp intergranular fracture surface along a quench crack in an experimental high-strength Cu-Ni-Sn-Pb alloy (after Felberbaum[125]).

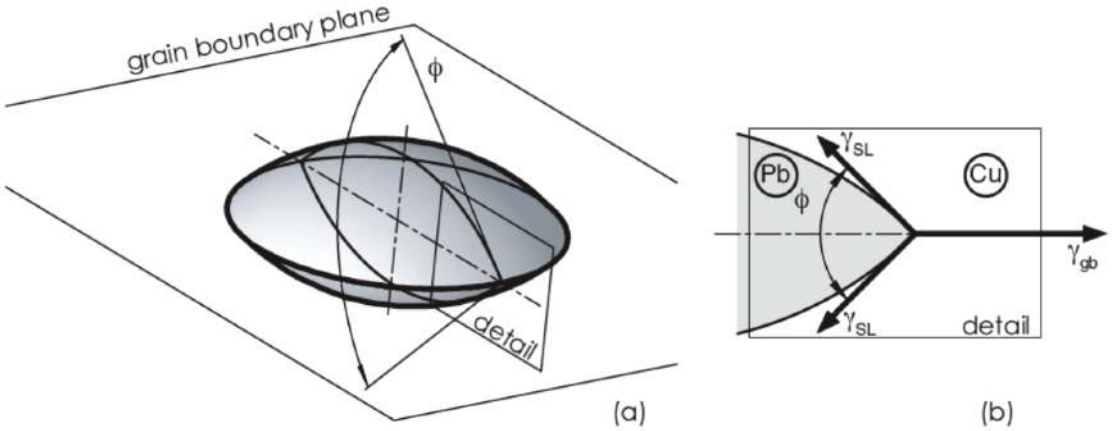

Figure 18 - Schematic view of an equilibrated lenticular inclusion situated along a planar grain boundary: (a) 3D view, and (b) detail: the cut is perpendicular to both the grain boundary plane and the triple line (after Felberbaum[125]).

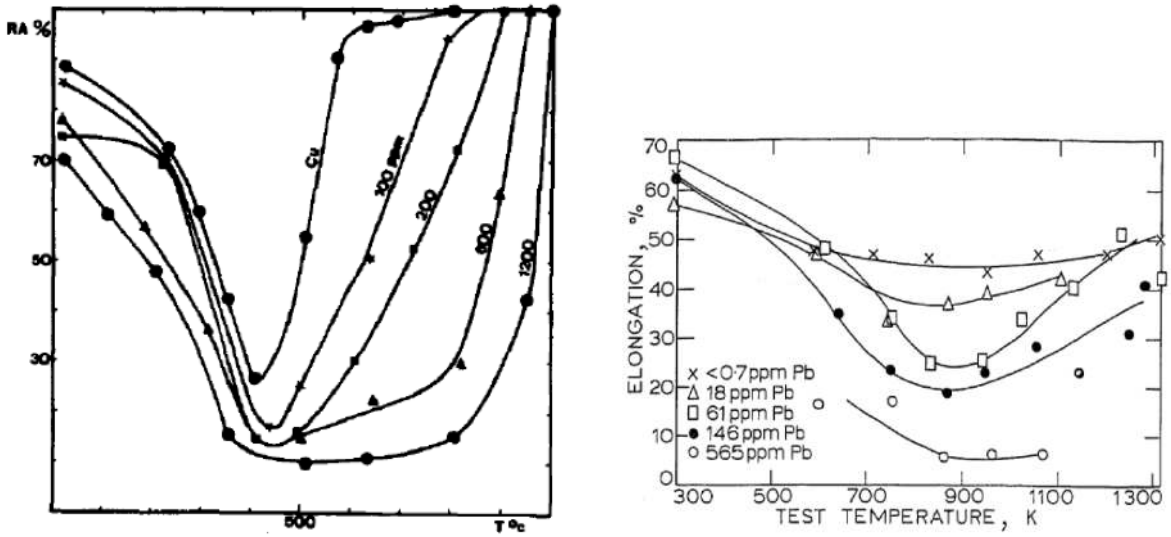

(a) (b)

Figure 19 - Effect of lead additions on ductility-temperature behaviour of OFHC copper (a) and high-purity Cu-10Ni alloy (b). Figure 19(a) reprinted from Sanchez Medina, Sangiorgi and Eustathopoulos [255] with permission from Elsevier Ltd. Figure 19(b) reprinted from Gavin, Billingham, Chubb and Hancock[10] with permission from Maney Publishers/the Institute of Materials.

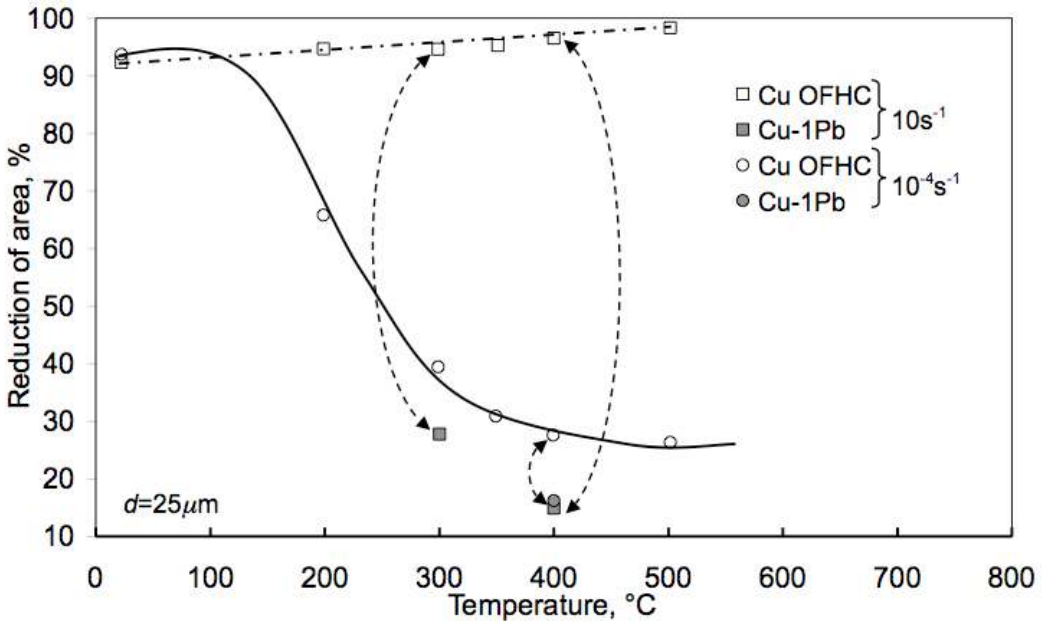

Figure 20 - Reduction in area of leaded and unleaded pure OFHC copper after elevated temperature tensile testing at two different strain rates; from Felberbaum[125]. Square symbols denote tests conducted at a strain rate of 10^{-4} s^{-1}, while round symbols are for tests conducted at 10 s^{-1}. Filled symbols are for Cu-1wt.%Pb. Arrows are added in order to help direct comparison between unleaded and leaded material under the same test conditions.

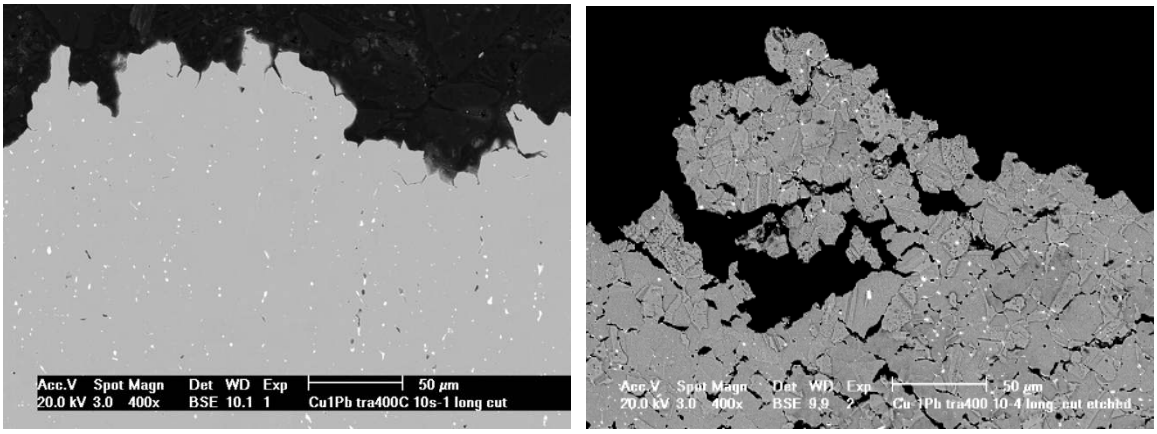

(a) Cu-1%Pb, , *RA*=15% (b) Cu-1%Pb, , *RA*=16%

Figure 21 - Longitudinal cuts across the tensile fracture surface of round bars of Cu-1wt.%Pb, tested at (a) 10 and (b) 10^{-4} s^{-1} (RA = Reduction in Area), denoting the presence of extensive damage at the lower strain rate, and of sharp intergranular fracture at the higher strain rate (from Felberbaum[125]; this figure is to be compared with Fig. 7).